AD-A050 743 POLYTECHNIC INST OF NEW YORK BROOKLYN DEPT OF PHYSICS F/G 20/8
COMPTON SCATTERING FROM ATOMS.(U)
MAR 77 L B MENDELSOHN, V SMITH N00014-75-C-0475
UNCLASSIFIED 77-1 NL

| OF |
AD
A050 743

END
DATE
FILMED
4-78
DDC

AD-A050 743

(1)

SECURITY CLASSIFICATION OF THIS PAGE (When Data Entered)

REPORT DOCUMENTATION PAGE

REPORT NUMBER	2. GOVT ACCESSION NO.	3. RECIPIENT'S CATALOG NUMBER
77-1		

TITLE (and Subtitle)	5. TYPE OF REPORT & PERIOD COVERED
Compton Scattering from Atoms	Annual (reprint)
	6. PERFORMING ORG. REPORT NUMBER

AUTHOR(s)	8. CONTRACT OR GRANT NUMBER(s)
Lawrence B. Mendelsohn, Vedene Smith	N00014-75-C-0475

PERFORMING ORGANIZATION NAME AND ADDRESS	10. PROGRAM ELEMENT, PROJECT, TASK AREA & WORK UNIT NUMBERS
Polytechnic Institute of New York Department of Physics Brooklyn, New York 11201	

CONTROLLING OFFICE NAME AND ADDRESS	12. REPORT DATE
Office of Naval Research Department of the Navy Arlington, Virginia 22217	March 1977
	13. NUMBER OF PAGES 37

MONITORING AGENCY NAME & ADDRESS (if different from Controlling Office)	15. SECURITY CLASS (of this report)
	unclassified
	15a. DECLASSIFICATION/DOWNGRADING SCHEDULE

16. DISTRIBUTION STATEMENT (of this Report)

Distribution of this document is unlimited

17. DISTRIBUTION STATEMENT (of the abstract entered in Block 20, if different from Report)

18. SUPPLEMENTARY NOTES

19. KEY WORDS (Continue on reverse side if necessary and identify by block number)

20. ABSTRACT (Continue on reverse side if necessary and identify by block number)

Chapter 5 in COMPTON SCATTERING (McGraw Hill, 1977) covers: Impulse Approximation; Momentum Distributions and Impulse Compton Profiles; Calculations of Impulse Compton Profiles for One Electron Models; Electron Correlation and Impulse Compton Profiles; Relativistic Profile Corrections; Comparison of Theory and Experiment for Free Atoms.

DD

Published in COMPTON SCATTERING (edited by B. Williams)
McGraw Hill 1977

ATOMS

L. Mendelsohn and V. H. Smith

5.1 THE IMPULSE APPROXIMATION

Following the historically significant papers of DuMond,[1,2] almost all Compton profile experiments have been analysed in the so-called 'impulse approximation'. It is only in this approximation that a simple relationship exists between the Compton profile $J(q)$ and the electron momentum density (EMD) of the bound state of the atom, molecule, or solid being probed. Recent review articles[3,4] have derived the impulse approximation from the Waller–Hartree theory[5] or from the time dependent operator formalism results first obtained by Eisenberger and Platzman[6] (see chapter 2). The authors of previous review articles seem to feel that 'while corrections to the impulse approximation can now be made, they tend to be small'[4] and that a 'laborious calculation of the final state wave function is unlikely to be necessary except for deeply bound core electrons, or for very accurate experimental data'.[3] It is the purpose of this first section to present a more straightforward derivation of the impulse approximation and to comment in more detail on the accuracy of this approximation.

5.1.1 Derivation of the impulse approximation

In the non-relativistic Schrödinger equation, the perturbation on an electron due to the presence of a magnetic field with vector potential A can be written

$$H' = \frac{e}{m_0 c}\,\mathbf{p}\,.\,\mathbf{A} + \frac{e^2}{2m_0 c^2}\,\mathbf{A}\,.\,\mathbf{A} \tag{5.1}$$

where p is the electron momentum, e is the electron charge, m_0 is the electron rest mass, and c is the speed of light. In a scattering process, the photon must suffer annihilation and then creation. By expanding A in creation and annihilation operators, it is clear that the scattering process is of order A^2. Thus, for a first order perturbation calculation the $\mathbf{p}\,.\,\mathbf{A}$ term contributes nothing. It is only in second order that this term can contribute to order A^2. However, if one assumes that the incident photon energy lies significantly above the ionization edge, the energy denominators in the second order perturbation theory expressions will make such $\mathbf{p}\,.\,\mathbf{A}$ contributions quite small. Some estimates of $\mathbf{p}\,.\,\mathbf{A}$ contributions have been made for the hydrogenic problem.[7,8] One usually considers only the A^2 term in first-order perturbation theory in the calculation of Compton scattering. The scattering process can be compared with the absorptive photo-electric effect where only the destruction of a

photon is required and only the $\mathbf{p} \cdot \mathbf{A}$ term is considered in lowest order perturbation theory (first order in A).

Using Fermi's golden rule for calculating the transition probability and cross-section along the lines of Schwinger[9] leads to the cross-section cited by Eisenberger and Platzman[6] for a single electron in an independent electron model

$$\frac{\mathrm{d}^2\sigma}{\mathrm{d}\Omega\,\mathrm{d}\omega} = \left(\frac{\mathrm{d}\sigma}{\mathrm{d}\Omega}\right)_{\mathrm{T}} \frac{\omega_2}{\omega_1} \sum_2 |\langle \psi_2 | \mathrm{e}^{i\mathbf{k}\cdot\mathbf{r}} | \psi_1 \rangle|^2 \delta(E_2 - E_1 - \omega) \tag{5.2}$$

where ω_1 and ω_2 are the incident and scattered photon energies respectively, $\omega = \omega_1 - \omega_2$, E_1 and E_2 are the initial and final electron energies respectively, $\mathbf{k} = \mathbf{k}_1 - \mathbf{k}_2$ is the scattering vector so that

$$k^2 = k_1^2 + k_2^2 - 2k_1k_2 \cos\phi \tag{5.3}$$

where $k_i = \omega_i/hc$ and ϕ is the scattering angle. ψ_1 and ψ_2 are the wave functions for the electron in its initial bound state and its final continuum state respectively. The Thomson cross-section for unpolarized incident radiation is given by

$$\left(\frac{\mathrm{d}\sigma}{\mathrm{d}\Omega}\right)_{\mathrm{T}} = (e^4/m_0^2c^4)\tfrac{1}{2}(1 + \cos^2\phi) \tag{5.4}$$

Eisenberger and Platzman[6] include a factor $(\omega_2/\omega_1)^2$ in their definition of $(\mathrm{d}\sigma/\mathrm{d}\Omega)_{\mathrm{T}}$ which modifies their eq. 6 to include the factor ω_1/ω_2 rather than ω_2/ω_1 in our eq. (5.2) above. The delta function in eq. (5.2) guarantees conservation of energy. In the general scattering case no conservation of momentum between the photon and electron is required as the nucleus itself may carry away momentum during the collision.

To derive the impulse result let us assume in the δ function that the electron can be treated as free (but moving) during the entire collision process. Before the collision let the electron have momentum $\mathbf{p}_1$ and after the collision momentum $\mathbf{p}_2$. Then

$$\begin{aligned} E_2 &= p_2^2/2m \\ E_1 &= p_1^2/2m. \end{aligned} \tag{5.5}$$

Conservation of momentum for this free electron case gives

$$\mathbf{p}_2 = \mathbf{p}_1 + \hbar\mathbf{k}; \quad p_2^2 = p_1^2 + 2\hbar\mathbf{k} \cdot \mathbf{p}_1 + \hbar^2k^2 \tag{5.6}$$

and the δ function becomes (see eq. (2.4))

$$\delta\{(2\hbar\mathbf{k} \cdot \mathbf{p}_1 + \hbar^2k^2 - \omega)/2m\} = \delta\left\{\frac{\hbar k}{m}\left[\frac{\mathbf{k} \cdot \mathbf{p}_1}{k} - \left(\frac{m\omega}{\hbar k} - \frac{\hbar k}{2}\right)\right]\right\}. \tag{5.7}$$

Within the impulse approximation ψ_2 is taken to be a plane wave

$$\psi_2(r) = \mathrm{e}^{i\mathbf{p}_2 \cdot \mathbf{r}/\hbar}. \tag{5.8}$$

The momentum space bound state wave function $\chi_1(\mathbf{p}_1)$ is the Fourier transform of the corresponding position space function so that

$$\chi_1(\mathbf{p}_1) = (2\pi\hbar)^{-3/2} \int \psi_1(\mathbf{r})\, e^{-i\mathbf{p}_1\cdot\mathbf{r}/\hbar}\, d^3r \tag{5.9}$$

and the sum over final states is

$$\sum_2 \rightarrow \int (2\pi\hbar)^{-3}\, d^3p_2. \tag{5.10}$$

Choosing $\mathbf{k}$ to lie in the z direction and using momentum conservation

$$\sum_2 |\langle\psi_1|e^{i\mathbf{k}\cdot\mathbf{r}}|\psi_2\rangle|^2\, \delta(E_2 - E_1 - \omega)$$

$$= \int d^3p_2 \left| (2\pi\hbar)^{-3/2} \int d^3r\, e^{i\mathbf{p}_1\cdot\mathbf{r}/\hbar}\, \psi_1(\mathbf{r}) \right|^2 \delta\left\{\frac{\hbar k}{m}\left[p_{1z} - \left(\frac{m\omega}{\hbar k} - \frac{\hbar k}{2}\right)\right]\right\}. \tag{5.11}$$

Defining

$$q = \frac{m\omega}{\hbar k} - \frac{\hbar k}{2} \tag{5.12}$$

eq. (5.11) reduces to

$$\int d^3p_2\, |\chi_1(\mathbf{p}_1)|^2\, \delta\left(\frac{\hbar k}{m}(p_{1z} - q)\right). \tag{5.13}$$

Noting that for ω_1, ϕ, and ω_2 (or ω) fixed, k is fixed as well, it follows from eq. (5.6) that the integral over d^3p_2 is equivalent to an integration over $d^3p_1 = dp_{1x}\, dp_{1y}\, dp_{1z}$. Making use of the properties of the δ function, eq. (5.13) becomes

$$\frac{m}{\hbar k} \int\int_{-\infty}^{+\infty} |\chi_i(p_{1x}, p_{1y}, q)|^2\, dp_{1x}\, dp_{1y} \tag{5.14}$$

which is equivalent to an integration over the plane in momentum space $p_{1z} = q$. For a momentum density which is spherically symmetric, it is convenient to rewrite eq. (5.14) in cylindrical coordinates from which it reduces to $(m/\hbar k)J(q)$ where

$$J(q) = 2\pi \int_{|q|}^{\infty} |\chi_1(p_1)|^2\, p_1\, dp_1. \tag{5.15}$$

Expressing p and q in atomic units of momentum $\hbar/a_0$, eq. (5.2) becomes the well known result for the Compton profile in the impulse approximation

$$\frac{d^2\sigma}{d\Omega\, d\omega} = \left(\frac{d\sigma}{d\Omega}\right)_T \frac{\omega_2}{\omega_1} \frac{ma_0^2}{\hbar^2} \frac{1}{ka_0} J(q). \tag{5.16}$$

The derivation has been presented in this much detail to bring out clearly all the approximations leading to the impulse result of eqs. (5.15) and (5.16), and also to serve as an introduction to the units commonly used in Compton work.

From the foregoing analysis it should be quite clear that the impulse approximation is equivalent to a photon scattering inelastically from a free electron gas with

a spherically symmetric (although this is not intrinsic to impulse) momentum distribution where both energy and momentum are conserved during the collision. The momentum density for any particular momentum in the free electron gas is obtained from the square of the Fourier transform of the initial bound state radial wave function. The energy-momentum conservation relations determine that for an incident photon with energy ω_1 scattering at any fixed $\mathbf{k}$ (ϕ and ω_2), contributions to the scattering from electrons with momenta $\mathbf{p}_1$ can occur only if the projection of $\mathbf{p}_1$ on the scattering vector $\mathbf{k}$ equals q. This can only occur if p_1 is greater than or equal to q.

DuMond[1] intuitively represented the atom as a free electron gas. Solving the energy-momentum conservation equations relativistically, he was able to show that because the electron moves with momentum $\mathbf{p}_1$ before the scattering, the wavelength of the scattered photon is Doppler shifted from the usual Compton result according to

$$\lambda_2 - \lambda_1 = \frac{h}{m_0 c}(1 - \cos\phi) + q\lambda^*/m_0 c \tag{5.17}$$

where

$$\lambda^* = (\lambda_1^2 + \lambda_2^2 - 2\lambda_1\lambda_2 \cos\phi)^{1/2} \tag{5.18}$$

and q is the projection of the initial momentum on the scattering vector as before. This result occurs after setting the initial electron energy to m_0c^2 and may not be immediately discerned from DuMond's papers since he defines λ^* and q slightly differently from the above. Since the λ^* term varies slowly over the profile, eq. (5.17) shows that λ_2 varies linearly with q. Equation (5.17) suggests that a large and negative q corresponds to a small λ_2 or a large ω_2 of the scattered photon, whereas a large and positive q corresponds to a large λ_2 or a small ω_2 of the outgoing photon, and a corresponding high energy for the ejected electron. From eq. (5.17), one can define q as

$$q = m_0 c l/\lambda^* \tag{5.19}$$

where

$$l = \lambda_2 - \lambda_1 - (h/m_0 c)(1 - \cos\phi) \tag{5.20}$$

represents the displacement in wavelength from Compton scattering from a free electron at rest. In his analysis DuMond first considered the scattering from a mono-energetic isotropic free electron gas with momentum p_1. It is clear from eq. (5.17) that such a gas would give rise to a flat intensity distribution with a width in λ_2 of $2p_1\lambda^*/mc$. It also follows that the area of this intensity band is proportional to the number of electrons with momentum p_1. Then considering a gas with a distribution in momentum and assuming scattering equally probable from any momentum, DuMond obtained the result of eq. (5.15) for the unnormalized intensity distribution. Of course this omits the slowly varying factors $\omega_2/\omega_1 k$ contained in the correct impulse result given in eq. (5.16). It is certainly a tribute to DuMond that his

intuitive approach brought out the most salient feature of the scattering, the Compton profile $J(q)$.

Simplified forms of λ^* such as

$$\lambda^* \simeq 2\lambda_1 \sin \tfrac{1}{2}\phi \tag{5.21}$$

$$\lambda^* \simeq 2(\lambda_1\lambda_2)^{1/2} \sin \tfrac{1}{2}\phi \tag{5.22}$$

have often been used in eq. (5.19). Use of eq. (5.21) will produce an error in q of order $[(\lambda_2 - \lambda_1)/\lambda_1]$ while eq. (5.22) leads to an error in q of order $[(\lambda_2 - \lambda_1)/\lambda_1]^2$. Since it introduces a first order error, one must be careful when using eq. (5.21) to determine the value of q, especially at large q values and for the case of large scattering angles and/or high incident energy photons. Phillips and Weiss[10] have calculated that for Mo $K\alpha$ radiation scattering at 90°, a q using λ^* defined by eq. (5.21) of 0·95 corresponds to a q determined by eq. (5.12) or (5.18) of 1·0. At a q value of about 8·0, the difference between the two q values rises to almost 10 per cent. Williams[11] has pointed out that the use of eq. (5.21) for typical X-ray wavelengths leads to a scale change of the order of 3 per cent and hence an error of about 3 per cent in the renormalized value of $J(0)$. From this discussion it should be clear that such approximations are not suitable for accurate work. It can be shown[12] that q (eq. (5.12)) determined from a non-relativistic approximation approach at the outset differs by terms of second order in $(\lambda_2 - \lambda_1)/\lambda_1$ from the q using the correct λ^* given by eq. (5.18).

In conclusion we note for the interested reader some other recent derivations and discussions of the impulse approximation.[13-15] Furthermore, in connection with the elegant derivation using a time-dependent operator formalism by Eisenberger and Platzman (see chapter 2), it has been pointed out by Benesch and Smith[15] that the use of the fundamental assumption

$$\exp(-[H_0, V]t^2/2) = 1 \tag{5.23}$$

in the many-electron case leads to an additional contribution proportional to

$$2\int d\mathbf{p}_1\, d\mathbf{p}_2\, \Gamma(\mathbf{k} + \mathbf{p}_1, \mathbf{p}_2 - \mathbf{k} \,|\, \mathbf{p}_1, \mathbf{p}_2)\, \delta(\omega - k^2/2 - \mathbf{k}\cdot\mathbf{p}_1) \tag{5.24}$$

where $\Gamma(\mathbf{p}_1, \mathbf{p}_2 \,|\, \mathbf{p}'_1, \mathbf{p}'_2)$ is the momentum space analogue of the spin-free two-particle density matrix in position space. It has been shown by Smith[16] that this contribution is negligible under normal experimental conditions but should be included when one integrates $d^2\sigma/d\Omega\, d\omega$ to obtain the total scattered intensity.

5.1.2 Accuracy of the impulse approximation

Returning to the basic eq. (5.2), it is quite clear that more realistic final state wave functions than plane waves can be used. In addition, E_1 in the delta function can be chosen to be the electron's binding energy. With these changes, analytic results have been obtained for the hydrogenic case. Results for the K-shell based on the analytic expression of Gummel and Lax[17] were obtained by Eisenberger and Platzman[6]

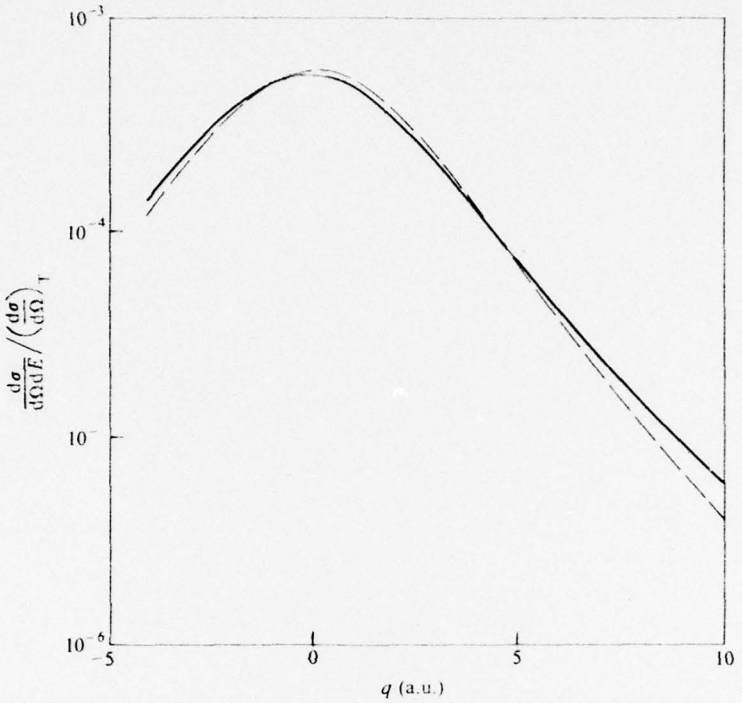

FIGURE 5.1
Comparison of EH and IH Compton profiles for a K-shell electron. $Z = 5$, $E_1 = 20$ keV, $\phi = 180°$. Solid line EH and dashed line IH.

and studied in some detail by Mendelsohn and Biggs.[18] It should be pointed out that Figure 3 in Ref. 6 which has now been reproduced in two review articles[3,4] is incorrect as it shows the 'correct' results lying above the impulse hydrogenic results at the profile centre. The error was fortunately corrected in Eisenberger's later analyses of experiments where a 1*s* core subtraction was needed. A correct comparison[18] of impulse hydrogenic and 'correct' hydrogenic is shown in Fig. 5.1 for a case similar to the one discussed in Ref. 6. Note in this fairly typical case that the curves cross twice. We shall refer to the correct results as the 'Exact Hydrogenic' (EH) results. Mendelsohn and Biggs[18] have shown analytically that for 1*s* electrons the impulse hydrogenic (IH) profile result at $q = 0$ lies above the EH result as

$$J_{IH}(0)/J_{EH}(0) \simeq 1 + 0{\cdot}145/(k^0 a_0/Z_{1s}^*)^2 \tag{5.25}$$

where k^0 is the value of the scattering vector at $q = 0$ and Z_{1s}^* is the effective charge in the 1*s* state. Clearly the correction is proportional to (binding energy)/(momentum transfer)^2. It should be noted that this statement is not in conflict with chapter 2 where it is stated that the impulse approximation is accurate to [binding energy/(momentum transfer)^2]^2. The latter comment was made with respect to the accuracy

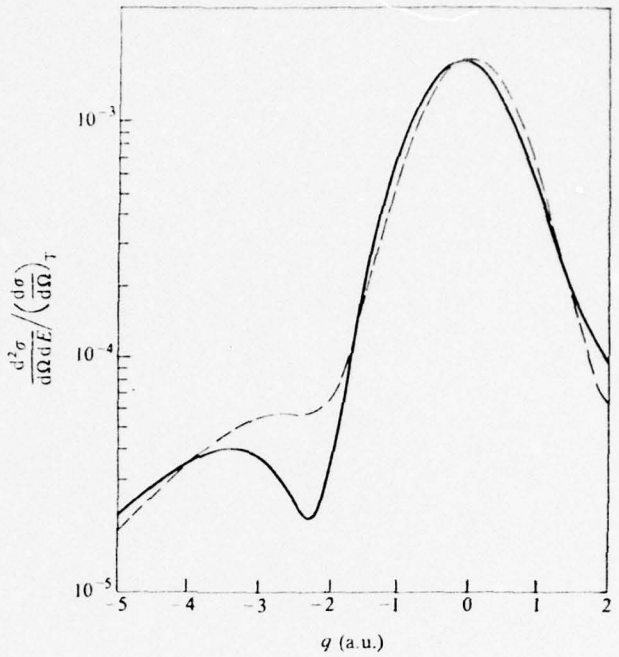

FIGURE 5.2
Compton scattering from a 2s electron. $Z = 5$, $E_1 = 20$ keV, $\phi = 180°$. Solid line EH and dashed line IH.

of the second moment of $S_1(k, \omega)$ while we are discussing the accuracy of $J(q)$ at $q = 0$.

EH L-shell calculation results and comparisons with experiment have been published in a series of papers by Mendelsohn, Bloch, and Smith.[19–21] These calculations used hydrogenic bound states and hydrogenic continuum states which are represented as confluent hypergeometric functions. Again it was shown analytically[19] for a 2s state that the IH profile lies above the EH profile at $q = 0$. Although no theorem was proven, it appears from calculations[20] for a filled 2p sub-shell, that the EH typically lies above the IH profile result at $q = 0$. An additional EH L-shell result[20] was that the 2s state can exhibit a secondary maximum on the negative q side of the profile as shown in Fig. 5.2 and occurs at approximately the value of q for which the IH result exhibits a plateau. This secondary maximum is more than an order of magnitude down from the primary central maximum. It appears to be related to the structure of the electron density in the original bound state wave function. Such secondary maxima in the 2s state have been predicted recently in *ion*-atom scattering calculations.[22]

Since the IH lies above the EH result at $q = 0$ for the 2s state and the IH lies below the EH result at $q = 0$ for a 2p state, there is a cancelling effect in the

calculation of a total L-shell Compton profile. Thus the EH correction to an impulse total profile is less than the corrections for the individual states. For the case of Mo $K\alpha$ radiation scattering through 170° from neon at $q = 0$ the $2s$ IH results lie 6·0 per cent above the EH results, whereas they lie 7·1 per cent below the EH results for a $2p$ (averaged) electron. Since there are 6 $2p$ electrons, a 2·39 per cent increase of EH over IH for the total L-shell profile is obtained. For Mo $K\alpha$ radiation scattering through 120° from aluminium, the individual $2s$ and $2p$ corrections are each about 20 per cent at $q = 0$, but the total L-shell EH $J(0)$ lies about 6 per cent above the IH value. In section 5.6 we will compare some of these results with experiments. Clearly L-shell corrections to impulse can be quite significant at conventional X-ray energies and scattering angles. Table 5.1 gives typical L-shell corrections for several

Table 5.1 L-shell Compton profile maxima $J(0)$ for several elements. IHF is the 'impulse' Hartree–Fock result which equals the 'impulse' hydrogenic result at $q = 0$ because of the way the Z^*'s have been chosen. $E_1 = 17{\cdot}374$ keV, $\phi = 155°$.

Element	$Z^*_{2s}(0)$	$Z^*_{2p}(0)$	$J_{EH}(0)$	$J_{IHF}(0)$	$\frac{J_{EH}(0)}{J_{IHF}(0)}$
Ne	5·99	4·96	2·609	2·548	1·024
Na	6·96	6·05	2·200	2·128	1·034
Mg	7·96	7·08	1·908	1·833	1·041
Al	8·91	8·11	1·692	1·615	1·048
Si	9·88	9·11	1·521	1·444	1·053
Ar	13·69	13·08	1·077	1·020	1·056

elements for Mo $K\alpha$ radiation. As one might expect, the corrections to impulse increase with increased binding (i.e. larger atomic number).

Since the EH approach to the correction of impulse profiles utilizes a screened hydrogenic model for both the ground and continuum states, both electron exchange and correlation are neglected. The use of a more realistic model for the evaluation of eq. (5.2) has been considered by DeCicco and collaborators[23,24] and Grossman and Mendelsohn.[25] These authors have used an atomic central field model potential due to Herman and Skillman (HS).[26] It employs the full Coulomb potential with the Slater local approximation to the non-local Hartree–Fock exchange and the so-called Latter r^{-1} tail. It corresponds to the choice of $\alpha = 1$ for the exchange parameter in the Hartree–Fock–Slater ($X\alpha$) model approach of Slater and co-workers which will be discussed in section 5.3 for impulse calculations.

In their method for calculation of exact Herman–Skillman (EHS) Compton profiles, Grossman and Mendelsohn use a modified version of the HS continuum wave function code of Manson.[27] They have found that of the order of 20 or more partial waves must be included to obtain convergence to three significant figures for a typical point on the profile. The method has been shown to give agreement with analytic EH results to more than three figures when a hydrogenic rather than a HS potential is used. This method can be used to calculate the Compton profiles of

electrons in any shell. Recently EHS calculations were carried out for the neon case mentioned above and were found to agree best with the experimental results over the whole profile. In addition an impulse calculation was performed using a ground state HS wave function. Again L-shell corrections to impulse of about 3 per cent were obtained at $q = 0$. Thus the magnitude of the correction for neon seems relatively independent of the theoretical bound state wave function approximation used. Another interesting preliminary result obtained with the partial wave HS method is that for 60 keV photons scattering from krypton, the corrections to the IHS $J(0)$ values for the individual orbitals may be of the order of a few percent. The correction to the impulse $J(0)$ result for the entire atom is significantly less than this because of cancellation effects.

As discussed in the next section, impulse Hartree–Fock–Slater ($X\alpha$) profiles are sensitive to the choice of the exchange parameter α, especially for outer orbitals. The close agreement of the EHS neon calculations with experiment may indicate that the choice of $\alpha = 1$ may have special advantages. Such a choice of α is known to pull in the spatial wave function too much as compared to a Hartree–Fock wave function. In the EHS calculation, this wave function choice may compensate in part for using the same potential for calculating the bound and continuum wave functions, (i.e., the frozen core approximation), and in part for ignoring correlation and relativistic effects. A discussion of the 'frozen core approximation' has been given by Currat *et al.*[23] and by Smith.[29] A further possible improvement to the EHS method could be the use of a more realistic value of α such as α_{CP} determined by Sabin and Smith[28] and discussed in section 5.3.

It has been asserted[6] that the impulse approximation gives very accurate results for large q since the electron is then ejected with high momentum and the plane wave representation becomes valid. This would certainly be the case if this were the only approximation inherent in the derivation of the impulse approximation. In the delta function the bound state electron has also been taken as free and it is not clear how this affects the asymptotic character of the results far out on the profile. Figure 5.1 for a K electron shows that the EH profile lies substantially above the IH profile if one goes out far enough in q.

5.2 MOMENTUM DISTRIBUTIONS AND IMPULSE COMPTON PROFILES

In the previous section, we have discussed the connection between the impulse Compton profile function $J(q)$, and the momentum distribution within the context of a one-electron model. As shown by Benesch and Smith,[15,30–32] one may generalize the relations (5.14) and (5.15) to reflect that $J(p_z)$ and $J(q)$ are one-dimensional projections of $\tilde{\rho}(\mathbf{p}) = \tilde{\gamma}(\mathbf{p}|\mathbf{p})$ where $\tilde{\gamma}(\mathbf{p}|\mathbf{p}')$ is the one-particle charge (or spin-free) density matrix in momentum space for the N-electron system. It is defined by eq. (5.26) in terms of the wave function in momentum space $\tilde{\chi}(X_1, X_2, \ldots, X_N)$ where $X_j = (\mathbf{p}_j, s_j)$ denotes the combined momentum and spin coordinates of electron j.

$$\hat{\gamma}(\mathbf{p}|\mathbf{p}') = \int_{s=s'} \chi^*(X', X_2, \ldots, X_N)\chi(X, X_2, \ldots, X_N)\,(\mathrm{d}X)_2. \tag{5.26}$$

In this equation $(\mathrm{d}X)_2$ denotes the combined operations of integration over the momentum coordinates and summation over the spin variables of electrons $2, 3, \ldots, N$. Just as the wave function in momentum space is related to the wave function in position space via the Dirac–Fourier transformation, so is $\hat{\gamma}(\mathbf{p}|\mathbf{p}')$ related to its position space analogue $\gamma(\mathbf{r}|\mathbf{r}')$ by[15]

$$\hat{\gamma}(\mathbf{p}|\mathbf{p}') = (2\pi)^{-3} \int \gamma(\mathbf{r}|\mathbf{r}')\, \mathrm{e}^{-i\mathbf{p}\cdot\mathbf{r}+i\mathbf{p}'\cdot\mathbf{r}'}\, \mathrm{d}\mathbf{r}\, \mathrm{d}\mathbf{r}'. \tag{5.27}$$

Thus the fundamental relations are

$$J(p_z) = \int\int_{-\infty}^{+\infty} \tilde{\rho}(p_x, p_y, p_z)\, \mathrm{d}p_x\, \mathrm{d}p_y \tag{5.28}$$

and

$$J(q) = \tfrac{1}{2} \int_{|q|}^{\infty} p^{-1} I(p)\, \mathrm{d}p \tag{5.29}$$

where the radial momentum distribution $I(p)$ is defined by

$$I(p) = p^2 \int \tilde{\rho}(\mathbf{p})\, \mathrm{d}\Omega_p. \tag{5.30}$$

These relationships clearly indicate that knowledge of $J(q)$ leads to information about the momentum distribution. However, it is logical to ask at this point why we should be interested in the momentum distribution except that it is accessible through the impulse approximation from the experimental Compton line shape. Can it add to the knowledge of electronic structure which we can derive from the familiar charge density $\rho(\mathbf{r}) = \gamma(\mathbf{r}|\mathbf{r})$, itself derivable from the experimentally measureable atomic form factor $F(\mathbf{s})$

$$F(\mathbf{s}) = \int \rho(\mathbf{r})\, \mathrm{e}^{i\mathbf{s}\cdot\mathbf{r}}\, \mathrm{d}\mathbf{r}. \tag{5.31}$$

This question is best answered by considering Fig. 5.3, where theoretical calculations[33] of $I(p)$, $J(q)$, $F(s)$, and $D(r)$ are presented for the ^4F state of atomic vanadium ($1s^2 2s^2 2p^6 3s^2 3p^6 3d^3 4s^2$). Here $D(r)$ is the radial charge density defined by

$$D(r) = r^2 \int \rho(\mathbf{r})\, \mathrm{d}\Omega. \tag{5.32}$$

The complementary and inverse nature of the information presented by $J(q)$ and $I(p)$ and by $F(s)$ and $D(r)$ is clearly seen. In the plot of $D(r)$ we can observe the peaks corresponding to the K, L, and M shells but lose sight of the N shell in the tails of the other shells. On the other hand, the radial momentum density $I(p)$ curve

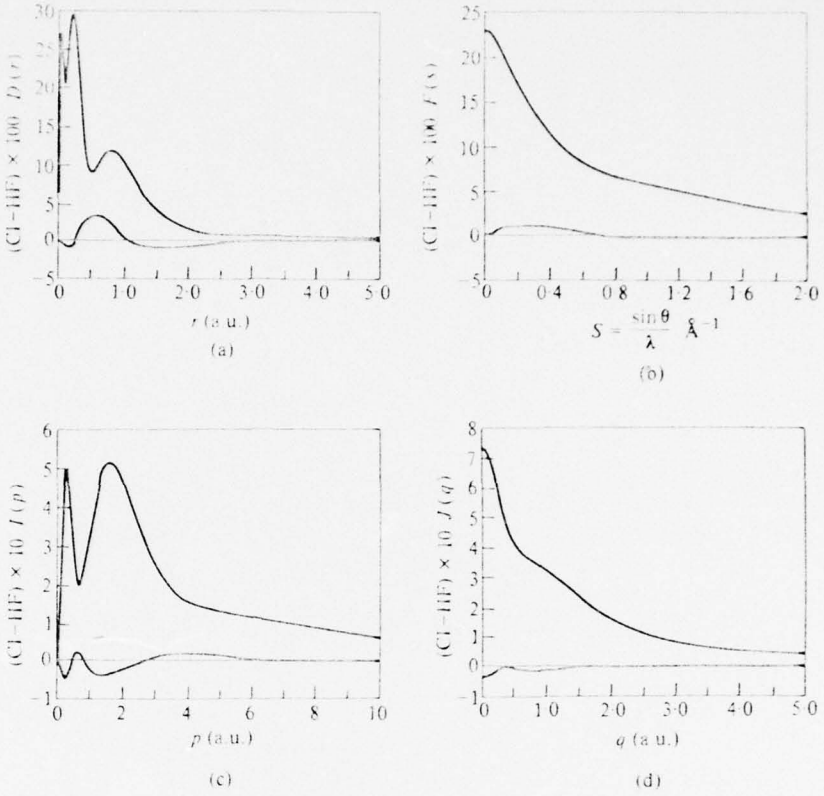

FIGURE 5.3
Comparisons of Hartree–Fock and correlated atomic functions for vanadium (^5F). (a) Radial charge density, $D(r)$. (b) Atomic form factor, $F(s)$. (c) Radial momentum density, $I(p)$. (d) Impulse Compton profile, $J(q)$.

shows the N and M shells respectively as p increases while the L shell is seen as the shoulder on the curve at 6 a.u. and the K shell is lost in the tails of the others. Consideration of the experimentally measurable quantities indicates that $F(s)$ does not reveal directly the shell structure while the noticeable changes in the slope of $J(q)$ distinguish the N and M shells while the core dominates the tails. The slope of $J(q)$ is simply

$$J'(q) = -\tfrac{1}{2}q^{-1}I(q). \tag{5.33}$$

It is clear that the charge and momentum densities do provide complementary information. One of the advantages of the Compton scattering technique lies in the fact that the contribution of the valence electrons is largest for small p (and q) where the experimental measurements are most accurate (see chapter 3).

Another aspect of the relation between $F(s)$ and $J(q)$ was shown by Benesch, Singh, and Smith,[32] namely that

$$F(\mathbf{s}) = \int \hat{\gamma}(\mathbf{p}|\,\mathbf{p}+\mathbf{s})\,d\mathbf{p}. \tag{5.34}$$

Thus $F(\mathbf{s})$ is a convolution of the entire one-particle density matrix in momentum space $\hat{\gamma}(\mathbf{p}|\,\mathbf{p}')$ while $J(q)$ is a one-dimensional projection of its diagonal component $\hat{\gamma}(\mathbf{p}|\,\mathbf{p})$. The stronger smoothing nature of the convolution may explain why correlation corrections to atomic form factors are usually smaller than those for Compton profiles which in turn are smaller than those for the momentum distribution.[34,35] Inspection of Fig. 5.3 confirms this. We shall return to the subject of correlation corrections in section 5.4.

It should be recalled that if one proceeds from the position space representation, determination of $\rho(\mathbf{r})$ and $F(\mathbf{s})$ requires only the diagonal component $\gamma(\mathbf{r}|\,\mathbf{r})$, while eq. (5.27) shows that the full $\gamma(\mathbf{r}|\,\mathbf{r}')$ is required for $\hat{\gamma}(\mathbf{p}|\,\mathbf{p})$.

5.2.1 Calculation of $\tilde{\rho}(\mathbf{p})$ and $J(q)$ for atomic systems

The preceding discussion makes clear that one way of calculating $\tilde{\rho}(\mathbf{p})$ and $J(q)$ is to use the prescription (5.26) to calculate $\hat{\gamma}(\mathbf{p}|\,\mathbf{p})$ from $\chi(X_1, X_2, \ldots, X_N)$. In turn, the wave function in momentum space may be obtained by Dirac–Fourier transformation of the position space wave function, i.e.,

$$\chi(X_1, X_2, \ldots, X_N) = (2\pi)^{-3N/2} \int \psi(x_1, x_2, \ldots, x_N) \exp\left(-i \sum_{j=1}^{N} \mathbf{p}_j \cdot \mathbf{r}_j\right) (\mathrm{d}x)_N \tag{5.35}$$

where $x_j = (\mathbf{r}_j, s_j)$ is the combined position and spin coordinate of electron j and $(\mathrm{d}x)_1$ has the analogous meaning to $(\mathrm{d}X)_2$ defined above. Since many position space wave functions are available for atomic systems or are easily calculable today, this transformation is the commonly followed procedure (or the equivalent transformation (5.27) of $\gamma(\mathbf{r}|\,\mathbf{r}')$) and will be discussed in some detail later in this section. However by writing the Schrödinger equation as an equation in terms of χ, it is possible to determine χ directly.

1. *Direct solutions for* χ. Two approaches may be considered. The first is a differential equation in momentum space where a simple replacement of x by $i\,\partial/\partial p_x$, etc., is made. Since the r^{-1} potentials involve differential operators, this approach is not a simple one. Hylleraas[36] did solve this differential equation for χ in the case of the hydrogen atom. In the second approach application of the Dirac–Fourier transformation to the position-space Schrödinger equation leads to an integral equation for χ. As an example, it takes the following form for the one-electron hydrogenic atom:

$$(p^2 - 2E)\chi(\mathbf{p}) = Z\pi^{-2} \int |\mathbf{p} - \mathbf{p}'|^{-2} \chi(\mathbf{p}')\,d\mathbf{p}'. \tag{5.36}$$

In this case it was solved exactly by Fock.[37,38] The analogous equation for the two-electron atomic problem was attacked by McWeeny and Coulson[39] and by

Henderson and Scherr[40] using an iterative method of solution. The difficulties which they encountered are one reason for the neglect of its use since then.

2. *Dirac–Fourier transformation of ψ or γ.* Although the direct solution method is dormant today due to the complexities involved in making it computationally tractable, McWeeny and Coulson[39] were led to consider it as a possible viable alternative to the Dirac–Fourier transformation. They commented that '... it proves impossible to transform to momentum space the most accurate wave functions in which electron correlation is adequately represented, the integrals involved being quite insuperable'.[39] Indeed, beside the difficulty of the integrals, it is certainly a laborious undertaking to take the total wave function in position space, compute its $3N$-dimensional Dirac-Fourier transform (eq. (5.35)), square the transform, and then integrate out the momentum space coordinates of the $N-1$ electrons (eq. (5.26)). In the case of an independent particle model wave function, i.e., one which is representable by a single Slater determinant,

$$\psi(x_1, x_2, \ldots, x_N) = (N!)^{-1/2} \begin{vmatrix} \psi_a(x_1) & \psi_a(x_2) & \cdots & \psi_a(x_N) \\ \psi_b(x_1) & \psi_b(x_2) & \cdots & \psi_b(x_N) \\ \vdots & \vdots & & \vdots \\ \psi_i(x_1) & \psi_i(x_2) & \cdots & \psi_i(x_N) \end{vmatrix} \tag{5.37}$$

one needs only to transform each individual spin orbital by means of eq. (5.9). Similarly in the case of a wave function which is expanded in terms of a set of spin orbitals, the transform of each individual spin orbital leads to χ expressed as the same expansion of Slater determinants but over the transformed set.

An alternative approach developed by Benesch and Smith[35] allows momentum distributions to be obtained from the most complicated position space wave functions wherein electron correlation is adequately represented. Since the one-particle charge density matrix $\gamma(\mathbf{r}|\mathbf{r}')$ may be expanded in terms of its eigenfunctions,[41,42] the natural orbitals (NO's) $\psi_i(\mathbf{r})$,

$$\gamma(\mathbf{r}|\mathbf{r}') = \sum_i \lambda_i \psi_i(\mathbf{r}) \psi_i^*(\mathbf{r}') \tag{5.38}$$

where λ_i is the occupation number of $\psi_i(\mathbf{r})$, knowledge of $\gamma(\mathbf{r}|\mathbf{r}')$ in terms of its NO's enables one to use eq. (5.26) to obtain $\hat{\gamma}(\mathbf{p}|\mathbf{p}')$ expanded in terms of the momentum space NO's,

$$\hat{\gamma}(\mathbf{p}|\mathbf{p}') = \sum_i \lambda_i \chi_i(\mathbf{p}) \chi_i^*(\mathbf{p}'). \tag{5.39}$$

Thus in the case of a $\gamma(\mathbf{r}|\mathbf{r}')$ of finite one-rank (i.e., the number of non-zero λ_i in eq. (5.38) is finite) one need only compute the Dirac–Fourier transform (eq. (5.9)) of each individual NO. This method has been used to calculate correlated profiles by a number of authors.

The case of wave functions (Hylleraas-type) which contain explicitly the inter-electronic coordinate r_{ij} is interesting. There are two approaches which may be used. One can expand the r_{ij} terms in a set of one-particle functions which in practice

are a truncated set.[43] The NO expansion is then available and the Benesch–Smith[15] procedure is applicable. Alternately, one may proceed to calculate $\gamma(\mathbf{p}|\mathbf{p}')$ directly as shown recently by Bonham[44] and Benesch.[45] Some of the integrals involved are not simple and require extensive computer time as shown in the calculations of Benesch for He.[45] Two earlier calculations[46,47] of the momentum distributions from Hylleraas-type functions for atomic helium have been reported. One of these[46] contained errors[45] while Hicks[47] chose wave functions which included only terms of the form r_{12}^2 whereas r_{12} terms are needed to properly represent the electron–electron cusp. The use of r_{12}^2 terms made the evaluation of the momentum distribution much simpler.

3. *Dirac–Fourier transformation of orbitals.* With the exception of the case of wave functions which explicitly contain the interelectronic coordinates r_{ij}, we have seen that the Dirac–Fourier transformation of the N-electron wave function ψ or the one-particle density matrix $\gamma(\mathbf{r}|\mathbf{r}')$ ultimately rests on the transformation of orbital functions from position to momentum space (eq. (5.9)). In the simplest case of atomic hydrogen, Podolsky and Pauling[48] transformed the position space solutions $\psi(\mathbf{r})$ to obtain the exact bound-state $\chi(\mathbf{p})$ with which the later direct calculations of Hylleraas[36] and Fock[37] were in agreement. The solutions which correspond to the familiar position space solutions

$$\psi(r) = f_{nl}(r)\, Y_{lm}(\theta, \phi) \tag{5.40}$$

are

$$\chi(p) = u_{nl}(p)\, Y_{lm}(\theta_p, \phi_p) \tag{5.41}$$

where $Y_{lm}(\theta, \phi)$ and $Y_{lm}(\theta_p, \phi_p)$ are the usual spherical harmonics in position and momentum space, respectively. This illustrates the isomorphic nature of the Dirac–Fourier transformation (eq. (5.9)), namely that s-orbitals transform to s-orbitals, p's to p's, etc. Instead of writing down the general solution[48,49] which involves Gegenbauer polynomials, we list the 1s and $2p$ solutions for future discussion and reference.

$$f_{1s}(r) = 2Z^{3/2} \exp(-Zr) \tag{5.42}$$

$$u_{1s}(p) = (32Z^5/\pi)^{1/2}(Z^2 + p^2)^{-2} \tag{5.43}$$

$$J_{1s}(q) = (8Z^5/3)(Z^2 + q^2)^{-3} \tag{5.44}$$

$$f_{2p}(r) = (Z^5/24)^{1/2} r \exp(-\bar{Z}r) \tag{5.45}$$

$$u_{2p}(p) = (4Z^7/3\pi)^{1/2} i^{-1} p(\bar{Z}^2 + p^2)^{-3} \tag{5.46}$$

$$J_{2p}(q) = (4Z^7/15)(\bar{Z}^2 + 5q^2)/(\bar{Z}^2 + q^2)^5 \tag{5.47}$$

where Z is the nuclear charge and $\bar{Z} = Z/2$.

In the case of a many-electron system, we assume that an orbital $\psi_j(r)$ such as a natural orbital or Hartree–Fock orbital may be written in the position space form of eq. (5.40) or in the more general case as a linear combination of such 'restricted' functions. For such atomic orbitals the radial function $f_{nl}(r)$ is usually

written as an expansion over a finite set of analytic functions or as a numerical tabulation. The momentum space orbital is of the form of eq. (5.41), i.e., $\chi_j(\mathbf{p})$ has the same angular dependence as $\psi_j(\mathbf{r})$ and the radial function $u_{nl}(p)$ is given by the symmetry-dependent transformation,

$$\begin{aligned} u_{nl}(p) &= (-i)^l \sqrt{2/\pi} \int_0^\infty j_l(pr) f_{nl}(r) r^2 \, dr \\ &= (-i)^l p^{-1} H_{nl}(p) \end{aligned} \tag{5.48}$$

where the Hankel transform $H_{nl}(p)$ involves a spherical Bessel function $j_l(r)$ of the order of the angular momentum quantum number l. In this case it is the Hankel transform of order $l + \frac{1}{2}$ of the function $rf_{nl}(r)$, i.e.,

$$H_{nl}(p) = \int_0^\infty [r f_{nl}(r)] J_{l+1/2}(pr)(pr)^{1/2} \, dr \tag{5.49}$$

where $J_{l+1/2}$ is the ordinary Bessel function. For a number of possible forms for $f_{nl}(r)$, the $u_{nl}(p)$ have been derived in the literature for various special cases and are discussed and tabulated quite generally, together with the associated $J(q)$ by Smith and Kaijser.[49] For atomic calculations, the commonly used functional forms for $f_{nl}(r)$ are the hydrogenic functions,[48] the nodeless Slater-type orbitals (STO)

$$f_{nl}(r) = [(2\alpha)^{2n+1}/\Gamma(2n+1)]^{1/2} r^{n-1} e^{-\alpha r} \tag{5.50}$$

and the Gaussian-type orbitals (GTO)

$$f_{nl}(r) = [2(2\alpha)^{n+1/2}/\Gamma(n+\tfrac{1}{2})]^{1/2} r^{n-1} e^{-\alpha r^2}. \tag{5.51}$$

In the case of orbitals which are either tabulated numerically or for which the analytical transform is not available, numerical techniques must be employed. The accurate numerical evaluation of Fourier sine and cosine transforms such as we have in eq. (5.48), is beset with difficulties due to the rapid oscillation of the integrand. As $p \to \infty$, sine and/or cosine functions oscillate with such rapidity that even in the case of radial functions $f_{nl}(r)$ that very rapidly approach zero as r approaches infinity, the transform is made up of an extremely large number of significant positive and negative contributions of nearly equal size that arise from the cycles of the trigonometric functions involved. It is for this reason that the results presented in several recent studies involving numerical transformation of atomic orbitals were lacking in the desired accuracy. The accurate evaluation of these transforms has been considered recently by Thakkar and Smith,[50] by Benesch[51] and by Thulstrup[52] with the former authors emphasizing the evaluation to controlled accuracy.

4. *Asymptotic and other properties of $I(p)$ and $J(q)$.* Certain moments of the momentum distribution defined by

$$\langle p^n \rangle = \int_0^\infty p^n I(p) \, dp \tag{5.52}$$

are of physical interest. The best known is $\langle p^2 \rangle$ which is twice the kinetic energy and by virtue of the virial theorem is just twice the negative of the total atomic energy. Inspection of the basic definition, eq. (5.29), shows that $1/2\ \langle p^{-1} \rangle$ is just $J(0)$, the peak value of the Compton profile, while $\langle p^0 \rangle$ is $N/2$. The operator, p^4, arises in the context of the relativistic Breit equation written in the Pauli approximation.[53] It is interesting to note that the possible integral moments $\langle p^n \rangle$ are confined to the range $-2 \leq n \leq 4$ for the exact wave function and that[15,54,55] for $0 \leq n \leq 4$,

$$\langle p^n \rangle = 2(n+1)\langle q^n \rangle \tag{5.53}$$

where $\langle q^n \rangle$ is the nth moment of the Compton profile function $J(q)$,

$$\langle q^n \rangle \doteq \int_0^\infty q^n J(q)\, \mathrm{d}q. \tag{5.54}$$

To understand these statements it is necessary to investigate the small and large p behaviour of $I(p)$ (or $\gamma(p\,|\,p)$) and similarly the small and large q behaviour of $J(q)$.

The expansion of $J(q)$ about $q = 0$ is

$$J(q) = J(0) - \pi\tilde{\rho}(0)q^2 - \tfrac{1}{4}\pi\tilde{\rho}''(0)q^4 - \cdots \tag{5.55}$$

and similarly

$$I(p) = 4\pi\tilde{\rho}(0)p^2 + \tfrac{1}{4}\pi\tilde{\rho}''(0)p^4 + \cdots. \tag{5.56}$$

Since the experimental measurements are the most accurate around the profile peak, *Bonham*[56] suggested that $\tilde{\rho}(0)$ and $\tilde{\rho}''(0)$ can be extracted from experimental $J(q)$ curves and compared with theoretical calculations. Use of eq. (5.56) in eq. (5.52) indicates that $\langle p^n \rangle$ would not exist for $n < -2$ unless $\tilde{\rho}(0)$ vanishes.

For large p, it may be shown that

$$I(p) = Cp^{-6} + O(p^{-8}) \tag{5.57}$$

and

$$J(q) = (C/12)q^{-6} + O(q^{-8}) \tag{5.58}$$

where[15,57,58]

$$C = 8\left\{4Z^2\left\langle \sum_i \delta^3(\mathbf{r}_i)\right\rangle + \left\langle \sum_{i<j} \delta^3(\mathbf{r}_{ij})\right\rangle\right\} \tag{5.59}$$

under the assumption that the wave function satisfies both the Kato electron–nuclear and electron–electron cusp conditions.[59,60] Both of these coefficients play roles in relativistic and radiative corrections to the energy.[53] This expression may be written alternately as

$$C = 8\{4Z^2\rho(0) + h(0)\} \tag{5.60}$$

where $\rho(0)$ is the charge density at the nucleus and $h(0)$ is the intracule pair function[61] evaluated at the electron–electron coalescence. Both of these contributions have been

tabulated for the two-electron atomic ions.[62,63] The data shows that the first term (the electron–nuclear contribution) in eq. (5.59) or (5.60) is the dominant one in this case. It is interesting to note that the so-called correlation contribution[64] to the tails of the profile does exist in the asymptotic region, but is probably not of the magnitude necessary to explain the older experimental data. However, it should be noted that for the uniform electron gas the electron–electron contribution is the only one present, while for the $s = N/2$ state of an atom it vanishes. For a wave function of finite one-rank such as produced by independent particle models and the method of superposition of configurations, the second term of eqs. (5.59) and (5.60) would not have appeared.[15]

Use of eq. (5.57) establishes that $\langle p^n \rangle$ does not exist for $n > 4$ unless c is zero. Equation (5.52) follows from eq. (5.54) by integrating the expression for $\langle q^n \rangle$ by parts

$$(n+1)\langle q^n \rangle = \left[q^{n+1} J(q)\right]_0^\infty - \int_0^\infty q^{n+1} J'(q)\, dq. \tag{5.61}$$

Since $J(q)$ vanishes as q^{-6} for large q, the first term is zero for $0 \leq n \leq 4$. Use of eq. (5.33) for $J(q)$ in terms of $I(q)$ in the second term completes the derivation. These sum rules (5.53) are a very useful method for checking the accuracy of calculated Compton profiles. It is recommended that in all calculations of $J(q)$ and $I(p)$ the internal consistency is checked by computing $\langle p^n \rangle$ and $\langle q^n \rangle$ at least for $n = 0$ and $n = 2$ which were probably already calculated in the position space representation as well.

5.3 CALCULATIONS OF IMPULSE COMPTON PROFILES FOR ONE-ELECTRON MODELS

5.3.1 Hartree–Fock

Since it is not possible to solve the Schrödinger equation exactly for systems containing more than a single electron, approximate methods for the determination of the wave function are used which are usually based on the energy variational principle. The simplest ansatz is that of the single-Slater determinant defined in eq. (5.37) or a linear combination of such determinants chosen so that the total wave function possesses the proper symmetry properties (L^2 and S^2) of the state in question. The orbitals involved will be solutions to the atomic HF equations

$$\begin{aligned} H_{\text{eff}}\phi_i &= \varepsilon_i \phi_i \\ H_{\text{eff}} &= -\tfrac{1}{2}\nabla^2 - Z/r + V_c + V_x \end{aligned} \tag{5.62}$$

where V_c is the Coulomb potential due to the electronic charge $\rho(\mathbf{r})$, V_x is the non-local exchange potential, and the orbitals $\phi_i(\mathbf{r})$ are assumed to be restricted to the form (5.40). Since H_{eff} depends on the N occupied orbitals $\{\phi_i(r)\}$, the solution of these equations was for many years a stumbling block in the theoretical description of atomic structure. As a result, the earliest calculations[65,66,67] of Compton profiles for many-electron atoms employed as crude approximations to the solutions of

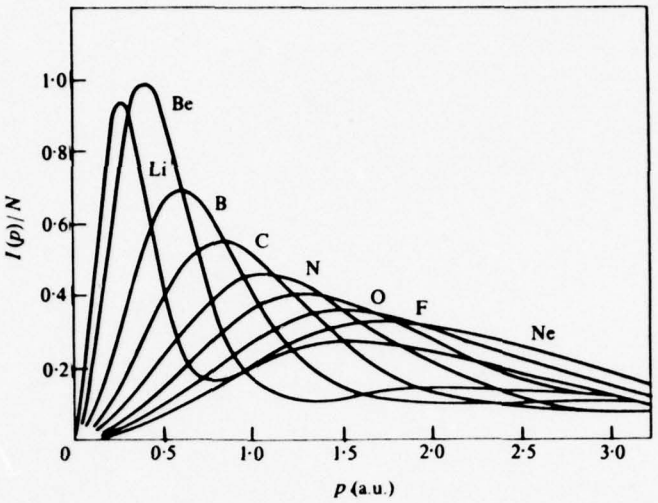

FIGURE 5.4
Radial momentum density $I(p)/N$ for the ground states of the first row atoms.

eq. (5.62), either hydrogenic or Slater-type orbitals with shielding factors chosen on the basis of Slater's rules[68] or similar criteria. However, many of these calculations were reported with $J(0)$ fixed to a common value rather than the profile area normalized to $N/2$ as expressed by eq. (5.52) for $n = 0$. The first extensive study was made by Duncanson and Coulson[69,70] who reported calculations for the neutral atoms from hydrogen to potassium ($Z = 19$) using STO's (eq. (5.49)) or with orbital basis functions[71] of the Morse–Young–Haurwitz type. They were the first to observe the momentum space shell structure illustrated in Fig. 5.4 for $I(p)/N$ for the first row atoms (Li–Ne) and which we discussed in connection with Fig. 5.3 for V. They noted that *s*-electrons give narrower or more compact $I(p)$ distributions than do *p*-electrons and were thus able to explain via the *aufbau* principle the successive expansion and broadening of the $I(p)$ curves observed in Fig. 5.3.

Table 5.2 Extensive tabulations of HF Compton profiles for neutral atoms

Authors	Wave function	Atoms (Z)	Relativistic
Weiss, Harvey, and Phillips[74]	Clementi[72] (STO basis)	Li(3)–Ge(32)	No
Benesch[80]	Numerical	As(33)–Yb(70)	No
Biggs, Mendelsohn, and Mann[79a]	Numerical	H(1)–Kr(36)	No
Biggs, Mendelsohn, and Mann[79a]	Numerical	Kr(36)–Nb(102)	Yes
Biggs, Mendelsohn, and Mann[79b]	Numerical	He(2)–Nb(102)	Yes

With the advent of modern computers, it has become possible to solve eq. (5.62) by the self-consistent-field (SCF) procedure either in terms of analytic basis functions[72] or numerically.[73] As a result, impulse Compton profiles of Hartree–Fock quality have been calculated in recent years by a number of authors.[30–32,74–81] The most extensive and useful tabulations[74,79,80] are listed and described in Table 5.2. The Compton profiles for the numerical Hartree–Fock wave functions should be considered as a reference standard for comparison of calculations made with either more elaborate wave functions or basis sets intended for use in molecular calculations. In the first four columns of Table 5.3 we have listed $J(q)$ for four Hartree–Fock quality wave functions[72,81,82] calculated by Smith, Brown, and Benesch[81,83] in order to indicate the effect of basis set quality.

Table 5.3 Comparisons of various correlated and Hartree–Fock impulse Compton profiles for boron (^2P)[a]

q (a.u.)	HF[b]	HF[b]	HF[c]	HF[d]	2CI[e]	Pol.[f]	FO[f]	187CI[f]
0·0	2·9924	2·9887	2·9889	2·9896	2·9507	2·9685	2·8878	2·8954
0·1	2·9135	2·9107	2·9110	2·9113	2·8757	2·8911	2·8187	2·8250
0·2	2·6918	2·6911	2·6912	2·6912	2·6648	2·6735	2·6224	2·6256
0·3	2·3684	2·3697	2·3695	2·3692	2·3545	2·3561	2·3314	2·3310
0·4	*1·9984*	*2·0006*	*2·0002*	*2·0000*	*1·9964*	*1·9929*	*1·9918*	*1·9885*
0·5	1·3118	1·3129	1·3127	1·3128	1·3236	1·3173	1·3413	1·3363
0·8	0·8432	0·8429	0·8432	0·8432	0·8574	0·8527	0·8779	0·8750
1·0	0·5788	0·5784	0·5786	0·5785	0·5903	0·5873	0·6056	0·6050

[a] Compton profiles were calculated by Smith, Brown, and Benesch.[81]
[b] Clementi.[72]
[c] Bagus-Gilbert.[82]
[d] Numerical.[81]
[e] 2*s*-2*p* Correlation.[117]
[f] *The density matrices of the Schaeffer–Harris functions*[114] *are from Brown and Smith.*[115]

5.3.2 Local density models

Because of the complexity of solving the Hartree–Fock equations (eq. (5.62)) which is especially due to the presence of the non-local exchange term V_x, there has been a long-standing interest in the development of local density models for the description of the electronic structure of atoms, molecules, and solids. Because the atomic Hartree–Fock equations are solvable as a routine matter today,[73] atoms represent an ideal test case for such models.

The Thomas–Fermi (TF) and Thomas–Fermi–Dirac (TFD) models have been applied with some degree of success, especially for heavier atoms. The corresponding momentum distributions and Compton profiles have been considered by several authors.[65,84–89] The TF model gives a profile of the wrong shape. The peak value is quite high in comparison with HF even for a heavier atom such as krypton. The value of $J(0)$ may be shown to be $CZ^{1/3}$ where C is approximately equal to 3·2. This wrong behaviour for small p is due to the r^{-6} asymptotic dependence of $\rho(r)$ in the TF model instead of the proper exponential decay. On the other hand the TFD method cuts $\rho(r)$ off after a finite distance and hence leads to a more realistic behaviour for small p and q.

As an outgrowth of the ideas of the Thomas–Fermi model,[87] there has been a great deal of attention paid in recent years to developing methods wherein the electronic potential energy is a local functional of $\rho(r)$.[90–92] A common feature of these models is the replacement in (eq. (5.62)) of the exchange potential V_x by

$$\begin{aligned} V_{x\alpha} &= \alpha V_{xs} \\ V_{xs} &= 4\left(3/(8\pi)\rho(r)\right)^{1/3} \end{aligned} \tag{5.63}$$

where V_{xs} was introduced by Slater[93] by consideration of the properties of the electron gas. A number of criteria have been suggested for the choice of the parameter α and have been studied from a number of viewpoints including momentum

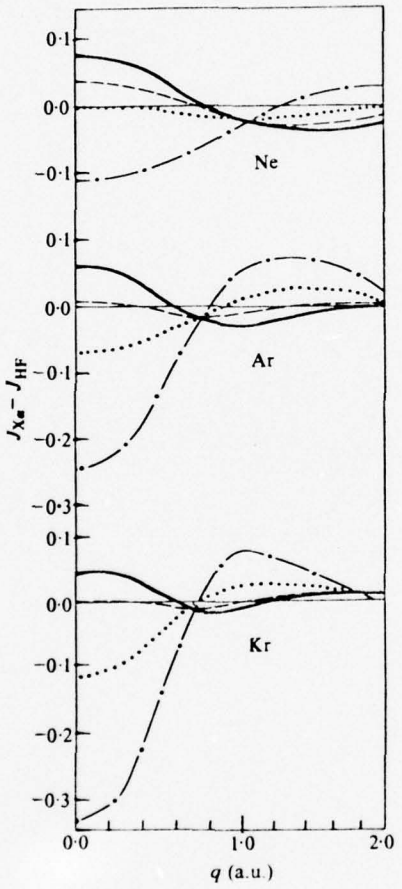

FIGURE 5.5
Difference between the $X\alpha$ and HF impulse Compton profiles for different choices of α. — · — · — $\alpha = 1$; ····· $\alpha = 0{\cdot}8$, - - - - - α_{VT}, ——— $\alpha = \frac{2}{3}$.

space properties.[28,35,94,95] It was found that the Compton profile was sensitive to the choice of α. In Fig. 5.5, the difference between $J_{x\alpha}(q)$ and J_{HF} is shown[94] for several choices of α including in decreasing magnitude of α: the original Slater value $\alpha = 1$, $\alpha = 0{\cdot}8$, the virial theorem value[96] α_{VT}, and the Gaspar[97]–Kohn–Sham[98] value of 2/3. It is seen for Ar and Kr that α_{VT} is the best choice of those illustrated, while for Ne there is a significant discrepancy. Since the choice of α_{VT} *emphasizes* $\langle p^2 \rangle$, it was suggested by Sabin and Smith[28] that a different criterion be employed for Compton profile studies which emphasizes $\langle p^{-1} \rangle$, namely α_{CP} should be chosen such that $J_{x\alpha_{CP}}(0) = J_{HF}(0)$, which is similar to the method introduced by Bloch and Mendelsohn[99] for the choice of atomic shielding parameters. In Table 5.4 we compare impulse Compton profiles and the relative percent difference for $\alpha = 2/3$, α_{VT} (0·7458), and α_{CP} (0·8032). It is seen that $J_{x\alpha_{CP}}$ is clearly in quite good agreement with J_{HF} for small q and in reasonably good agreement for a larger range.

In addition to the replacement of V_x by $V_{x\alpha}$ there has been much interest[88,91,97] in its replacement by various exchange and correlation potentials V_{xC} based again on electron gas considerations. We note that several authors[88,95] have calculated $I(p)$ and $J(q)$ from orbitals determined from different V_{xC}'s.

Table 5.4 Impulse Compton profiles[28,95] for various local exchange potentials for neon (^1S). Δ gives the difference from the HF value

q (a.u.)	$X\alpha 2/3$	Δ(%)	$X\alpha_{VT}$	Δ(%)	$X\alpha_{CP}$	Δ(%)	HF
0·0	2·8088	−3·0	2·7699	−1·5	2·7279	0·0	2·7279
0·5	2·5631	−2·0	2·5358	−0·9	2·5053	0·3	2·5131
1·0	1·8684	1·1	1·8695	1·0	1·8696	1·0	1·8889
2·0	0·7510	2·6	0·7616	1·2	0·7735	−0·3	0·7709

5.4 ELECTRON CORRELATION AND IMPULSE COMPTON PROFILES

Since accurate Hartree–Fock (HF) calculations for atomic states have become available in recent years, it is now possible to test the adequacy of the HF model for the description of electronic properties. HF-theory has been found to reproduce some expectation values of physical interest quite well, but for others it is not sufficiently accurate. As an example of the latter category, one may cite the electron affinity where for atomic oxygen the HF value is of the wrong sign. The problem of the difference between the HF and the exact non-relativistic prediction is called the *correlation problem*. It was originally formulated for the correlation energy,[100] namely the difference between the exact (non-relativistic) and the restricted Hartree–Fock (RHF) energy, i.e.,

$$E_{corr} = E_{exact} - E_{RHF} \tag{5.64}$$

Since this error is a small fraction of E_{RHF}, it is usually only in questions involving energy differences where the correlation energy is important.

One of the reasons for the accuracy of the HF energy is expressed by Brillouin's theorem[101] that E_{HF} and E_{exact} agree to second order. Similarly the Moller–Plesset theorem[102,103] indicates that the HF expectation values of one-electron operators should be correct to second order as well. The magnitude of this correction would be dependent on the nature of the operator and the state involved. In addition it is formulated for the HF model without restrictions rather than the RHF model which is commonly used.

Weiss[104] was probably the first to inquire about the possible effects of electron correlation on momentum distributions and Compton profiles. He felt that atomic HF momentum densities would probably not be as accurate as the HF atomic form factors which our previous discussion of eq. (5.34) supports. Calculations are now available at both the correlated and RHF level for the lighter atoms (He–Ne). In the case of helium[39,45,105] the data in Table 5.5 indicates that the HF and both

Table 5.5 Comparison of theoretical impulse Compton profiles for helium (^1S)

q (a.u.)	HF[30,45]	MCHF[30,105]	Corr.[45]
0·0	1·0705	1·068	1·0685
0·1	1·0568	1·055	1·0545
0·2	1·0172	1·015	1·0143
0·3	0·9557	0·954	0·9512
0·4	0·8782	0·876	0·8737
0·5	0·7911	0·788	0·7859
0·6	0·7004	0·698	0·6951
0·7	0·6112	0·609	0·6060
0·8	0·5271	0·525	0·5225
0·9	0·4251	0·449	0·4465
1·0	0·3820	0·381	0·3818

of the correlated profiles therein are in quite good agreement with a slight flattening of the profile because of electron correlation. Similar results were found for Li^+ and other two-electron ions.[31] Comparison of the HF and correlated $I(p)$ values for Li calculated by Benesch and Smith[32] indicates discrepancies of the order of 2–3 per cent while the Compton profile was more accurate. The maximum discrepancies for $J(q)$ occurred at the peak, 2·5928 (RHF) versus 2·5743 (correlated), a difference of 0·75 per cent. The atomic form factors[106] were in their turn even more accurate, illustrating the comparative smoothing nature of the convolution (eq. (5.34)) and the integration (eq. (5.29)) involved. The largest discrepancies for $I(p)$ and $J(q)$ occurred in the valence or L-shell region while in the K-shell region they were very small as in the case of Li^+ mentioned above.

Subsequently Benesch and Smith[107] and Naon and Cornille[108] examined beryllium (^1S). Both investigations revealed very large correlation effects in $I(p)$ and $J(q)$ which were primarily in the L-shell region. There was a decrease of approximately 7 per cent in the magnitude of $J(0)$ due to electron correlation. The

Table 5.6 Comparison of $J(0)$ values for several neon (^1S) wave functions[a]

Wave function	$J(0)$	$-E$
RHF (Clementi)	2·7279	128·5470
RHS (Bagus-Gilbert)	2·7257	128·5471
AH-MCHF[c]	2·7371	128·8016
CI (VHS)[d]	2·7245	128·8767
CI (VHS-scaled)[e]	2·7282	128·8770
BGI[f]	2·7340	[b]

[a] All calculations except BGI are from Smith and Brown.[109]

[b] The energy was not given in Ref. 108. It is only stated that 98 per cent of the correlation energy was recovered. For comparison, CI (VHS) and AH-MCHF yield 89 and 67 per cent respectively.

[c] The MCHF wave function of Ahlrichs and Hinze[112] which included only L-shell correlation. It should be noted that another calculation reported in the literature[78] used an incorrect version of this wave function.[113]

[d] The full second order CI of Viers, Harris, and Schaeffer.[112]

[e] Scaled to satisfy the virial theorem in Ref. 109.

[f] *Profile calculation* of Naon and Cornille[108] using Nesbet's Bethe–Goldstone increment method to treat L-shell correlation only.

cause of the discrepancy could be identified as being due to the near-degeneracy of the $1s^22s^2$ and $1s^22p^2$ configurations.

The calculations on atomic neon by Smith and Brown[109] and Naon and Cornille[108] showed that for this well-closed shell system, electron correlation played a very minor role in determining the Compton profile. This is seen by comparing the $J(0)$ values which are tabulated in Table 5.6. It should be observed that all the correlated values for $J(0)$ with the exception of one are larger than the HF value and hence provide a counter-example to the conjecture that

$$J(0)_{HF} > J(0)_{corr} \tag{5.65}$$

This conjecture which is based on the virial theorem originated with McWeeny and Coulson.[38] It was suggested in recent years by Brown and Smith[109,110] and was satisfied by calculations for He,[30,45,105] Li,[32] Be,[107,108] B,[81] and H_2.[110] However, recent calculations for H_2O[111] which is isoelectronic with neon, also contradict (5.65).

We note that the one calculation in Table 5.6 which obeyed eq. (5.65), did not satisfy the virial theorem but when scaled to do so no longer satisfied the conjecture. A study of atomic boron (^2P) by Smith, Brown, and Benesch[81] revealed that correlation flattened the $J(q)$ curve with the largest deviation (3·23 per cent) occurring for $J(0)$. Here again, the effect of electron correlation on $J(q)$ and $I(p)$ was largest in the L-shell region and relatively minor for the core (Fig. 5.6).In order to isolate the particular types of electron correlation which are important for describing $I(p)$ and $J(q)$, Smith, Brown, and Benesch[81] reported calculations for a series of wave functions which were carefully constructed by Schaeffer, Klemm, and Harris[114,115] to successively include the contributions in the Sinanoğlu[116] decomposition of the exact wave function into orthogonal parts

$$\Psi_{\text{exact}} = \Phi_{\text{RHF}} + \chi_{\text{INT}} + \chi_{\text{F}} + \chi_{\text{EXT}} \tag{5.66}$$

where Φ_{RHF} is the RHF configuration and the remaining terms represent various types of orbital substitutions with respect to it. χ_{INT} includes the *internal* correlation contributions, i.e., those double orbital substitutions where both substituted orbitals belong to the open shell (the $2s$–$2p$ shell in our case). χ_{F} includes *orbital polarization* and *semi-internal* contributions. The latter are doubly substituted configurations,

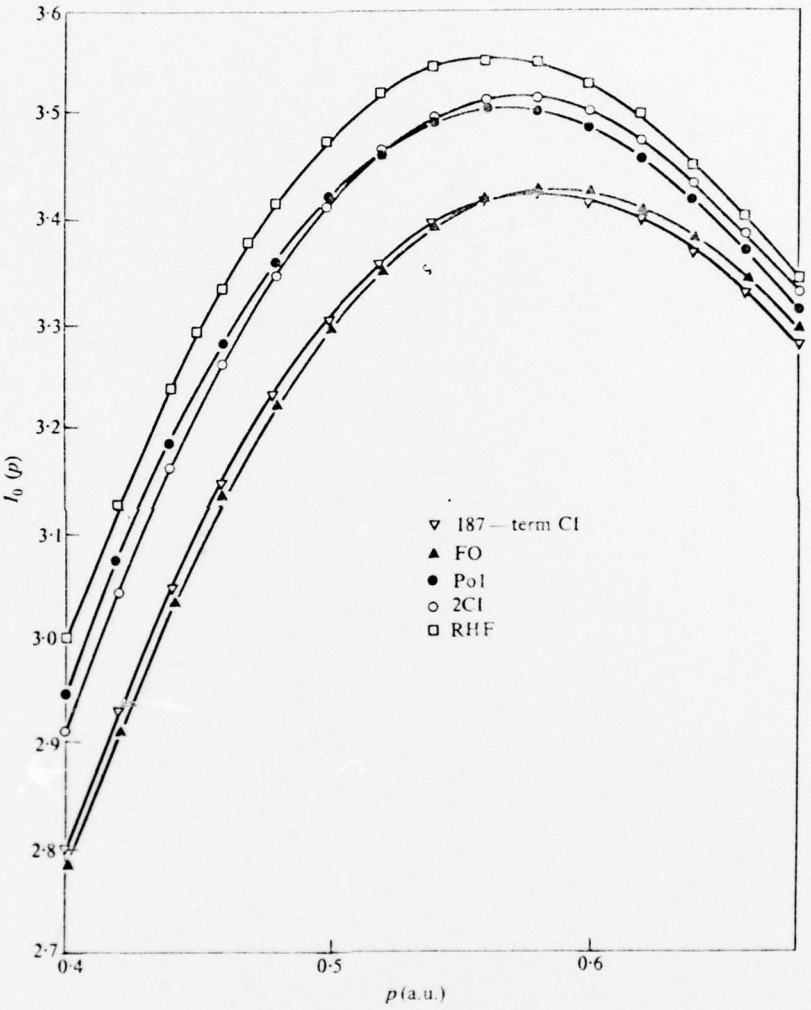

FIGURE 5.6
Comparison of Hartree–Fock and correlated momentum distributions $I(p)$ around the L-shell peak for B (^2P).

where only one of the substituted orbitals belongs to the open shell. The remaining term χ_{EXT} contains the remainder of the wave function including the *external* substitutions where all of the substituted orbitals are outside the open shell.

The Compton profiles corresponding to these correlated wave functions are included in Table 5.3. The 2CI wave function[117] consists of $\Phi_{RHF} + \chi_{INT}$, i.e., the two configurations $1s^2 2s^2 2p$ and $1s^2 2p^3$ while the 'Pol.' wave function included $\chi_{RHF} + \chi_F$ and the FO (first order[114] or charge-density[116]) wave functions consist of $\Phi_{RHF} + \chi_F + \chi_{INT}$. The 187-term CI includes most of the same contributions as the FO function plus some of the external contributions. Inspection of the table shows that the latter two functions are in very good agreement while the 2CI and Pol. functions each account for approximately half of the discrepancy at the peak. Smith, Brown, and Benesch[81] concluded that inclusion of the *internal* orbital polarization and *semi-internal* correlation effects in the valence shell is necessary to adequately describe the Compton profile for open-shell states while the *external* correlations play only a minor role. Since the *internal* and *semi-internal* contributions are absent for well-closed shell states, the reported accuracy of RHF for helium (^1S) and neon (^1S) is understood.

The most recent study is that of Munch and Davidson[33] for vanadium (^4F). Inspection of Fig. 5.3 shows that the correlation contribution is mainly in the valence region with a flattening of the profile in agreement with the conjecture of eq. (5.65).

5.5 RELATIVISTIC PROFILE CORRECTIONS

In this section we will discuss the effects of using a relativistic Hartree–Fock spinor wave function on the momentum density and impulse Compton profile. We will not touch upon the important question of a correct formalism relating the scattering cross-section to the impulse Compton profile for high incidence energy γ-ray photons scattered at any angle except to state that it has recently been reported by Ribberfors[118] (see also chapter 2).

5.5.1 Relativistic Hartree–Fock formalism

Relativistic Hartree–Fock impulse profile calculations have been reported in a series of papers by Mendelsohn, Biggs, and Mann.[79,119,120] The wave functions used were Mann's numerical relativistic Hartree–Fock wave functions.[121] These were obtained by solving the Dirac equations self-consistently taking all the two-particle interactions as Coulombic. In the relativistic central field Hartree–Fock case a particular n,l orbital (except for s orbitals) splits into two orbitals, one with $j = l + \frac{1}{2}$ and one with $j = l - \frac{1}{2}$. For either of the nlj orbitals, the four component spinor may be expressed in terms of only two radial components: $G_{nlj}(r)$, a large component which looks very much like the non-relativistic radial wave function for orbitals of small atoms, and $F_{nlj}(r)$, a small component. In terms of these components, the wave function normalization condition may be taken as

$$\int_0^\infty \{(G_{nlj}(r))^2 + (F_{nlj}(r))^2\} r^2 \, dr = 1 \tag{5.67}$$

The two components of the spinor which contain $G(r)$ are multiplied by spherical harmonics of order l. The two components of the spinor which contain $F(r)$ are multiplied by spherical harmonics of order $l+1$ for the $j = l + \frac{1}{2}$ case and of order $l-1$ for the $j = l - \frac{1}{2}$ case. Taking the Fourier transforms of the individual spinor components, the momentum wave function spinor can also be written in terms of two radial momentum components $\chi^G_{nlj}(p)$ and $\chi^F_{nlj}(p)$, where

$$\chi^G_{nlj}(p) = (2/\pi)^{1/2} \int_0^\infty G_{nlj}(r) j_l(pr) r^2 \, dr \tag{5.68}$$

and

$$\chi^F_{nlj}(p) = (2/\pi)^{1/2} \int_0^\infty F_{nlj}(r) j_{l+i}(pr) r^2 \, dr \tag{5.69}$$

where $i = 1$ for $j = l + \frac{1}{2}$ and $i = -1$ for $j = l - \frac{1}{2}$ and $j_l(pr)$ is a spherical Bessel function of the first kind. Finally the impulse profile is calculated from

$$\begin{aligned} J_{nlj}(q) &= \tfrac{1}{2} \int_q^\infty |\chi_{nlj}|^2 \, p \, dp \\ &= \tfrac{1}{2} \int_q^\infty \{(\chi^G_{nlj}(p))^2 + (\chi^F_{nlj}(p))^2\} p \, dp \end{aligned} \tag{5.70}$$

where the factor $\frac{1}{2}$, rather than 2π, comes from the normalization of G and F in eq. (5.67). A discussion of the numerical procedures employed to evaluate the integrals may be found in Ref. 79 (see section 5.2.1(3)). In addition a complete set of relativistic Hartree–Fock Compton profiles for the individual orbitals of all free atoms with $Z \geq 36$ is given in this reference.

5.5.2 Relativistic corrections to the Compton profile

The most interesting result of the relativistic calculations is that relativistic effects on outer electron, and therefore total, Compton profiles are much larger than one would expect *a priori*. The orbitals which contribute significantly at the profile centre are the outer electron atomic orbitals. One does not ordinarily think of these orbitals, where the electrons are moving comparatively slowly, as being affected very much by relativistic effects. On the other hand one expects the relativistic spatial wave functions of rapidly moving electrons in the inner orbitals of heavy atoms to be pulled in considerably when compared to non-relativistic wave functions. This pulling in of the relativistic electron density can be understood simply from considering the mass–velocity effect as a perturbation to the non-relativistic Hamiltonian. As such it has the same sign as the attractive nuclear potential[53] and therefore pulls in the electron wave function so that it is larger nearer the nucleus. Since a more sharply peaked inner electron spatial wave function leads to a flatter momentum space wave function,

and Compton profile, we expect a relativistic wave function to give a flatter Compton profile (lower in the centre, higher in the tails) than a non-relativistic wave function. However it is clear at once that if the inner 1s, 2s, and 2p orbitals are affected significantly by including relativistic effects, outer *s* and *p* orbitals may also be significantly altered because of orthogonalization (outer *s* to inner *s*, outer *p* to inner *p*).

Thus in lead a 1s electron shows a relativistic decrease in $J(0)$ of 18·7 per cent. Because its wave function has been altered significantly due to orthogonalization to the inner *s* states, a relativistic 6s electron exhibits a decrease in $J(0)$ of 13·9 per cent. These percentages are based on a comparison of profiles calculated with relativistic and non-relativistic Hartree–Fock wave functions. To see this clearly the non-relativistic (dashed line) and relativistic (solid line) Hartree–Fock electron charge and momentum densities for the 4s orbital of lead are compared in Fig. 5.7 and Fig. 5.8.

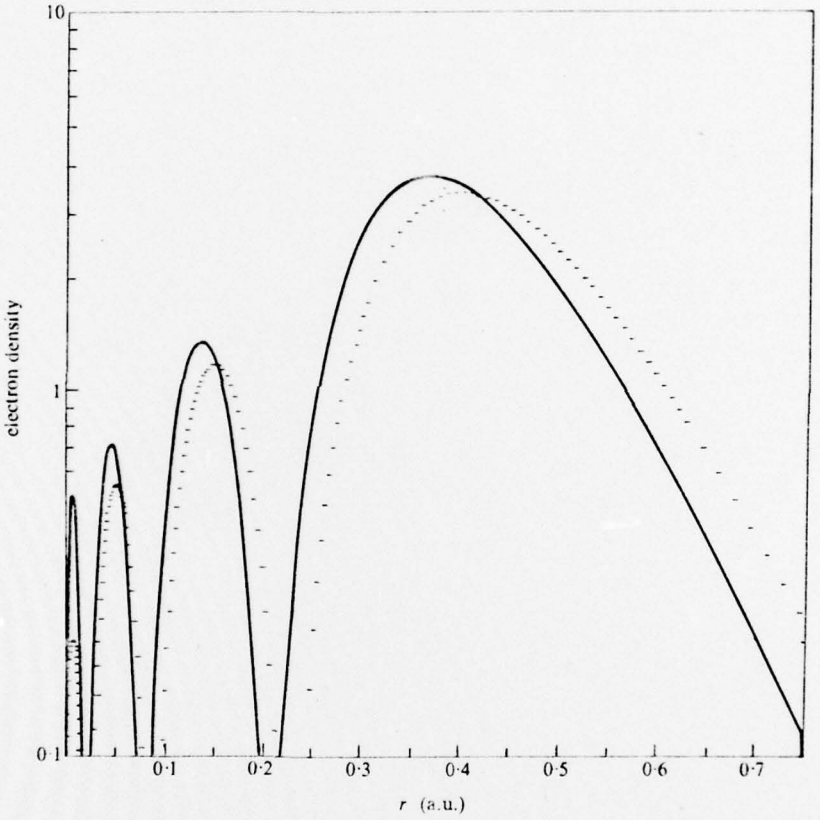

FIGURE 5.7
Comparison of Hartree–Fock (- - - -) and relativistic Hartree–Fock (———) electron densities for the 4s state of lead.

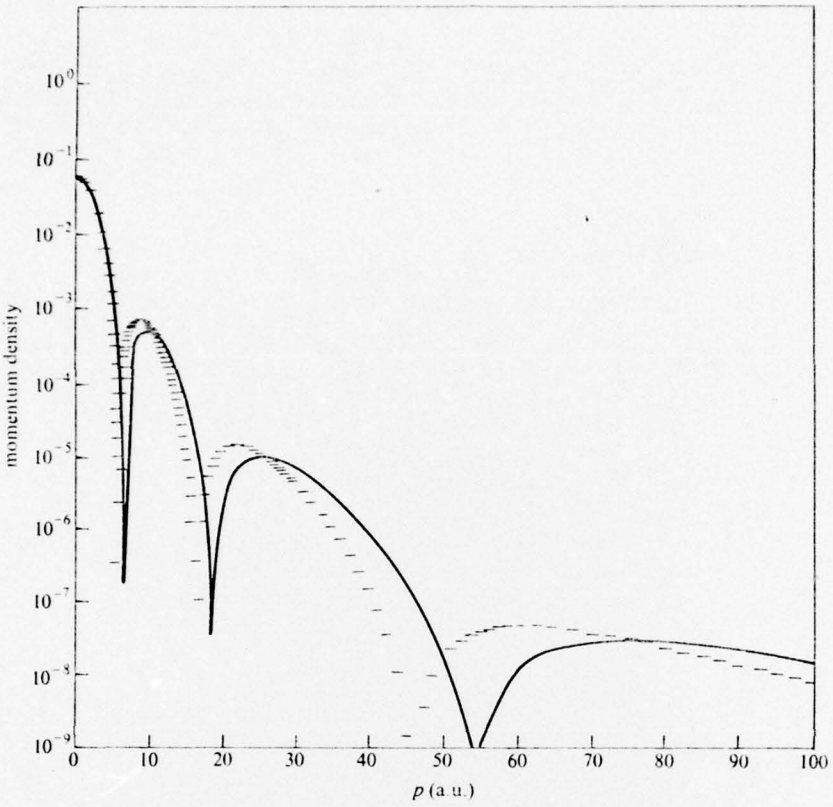

FIGURE 5.8
Comparison of Hartree–Fock (- - - -) and relativistic Hartree–Fock (———) momentum densities for the 4*s* state of lead.

Clearly the relativistic pulling in effect is quite large. Another difference not shown in the figure, is that the relativistic electron density does not exhibit nodes since the F and G components do not go to 0 at the same point. A similar type of comparison for the $6p$ electron of lead again shows a surprisingly large relativistic decrease in $J(0)$ of 9·52 per cent. In lead, as in other materials, relativistic flattening effects for d and f electrons are negligible for the most part. When the $J(0)$ values for all the orbitals of lead are added up, one finds a relativistic decrease of the total profile of 5·24 per cent at the profile centre. Since these relativistic profile calculations were performed within the impulse approximation using normalized Dirac spinor wave functions, the normalization condition on the profile of any orbital

$$2\int_0^\infty J(q)\,\mathrm{d}q = 1 \tag{5.71}$$

is maintained. This condition insures that the relativistic $J(p_z)$ out on the wings will lie higher than the non-relativistic profile result. To give the reader some estimate of relativistic flattening results for smaller atoms, we cite the results for the rare gases: for argon ($Z = 18$), a relativistic decrease in the total $J(0)$ of 0·187 per cent is found; for krypton ($Z = 36$), a decrease of 0·712 per cent is obtained; for xenon ($Z = 54$), the effect is 1.47 per cent.

5.6 COMPARISON OF THEORY AND EXPERIMENT FOR FREE ATOMS

X-Ray Compton scattering experiments using Mo $K\alpha$ (17·374 keV) and Ag $K\alpha$ (22·163 keV) sources have been performed by Eisenberger on helium[105] and neon.[122] γ-Ray experiments with a 160 keV ^{123m}Te source have been made by Eisenberger and Reed[123] on helium, argon, and krypton. Both experiments on helium were found to be in very good agreement with impulse Hartree–Fock profile calculations, a not surprising result since correlation, binding, and relativistic corrections are quite small for helium. The γ-ray data for argon and krypton was subsequently re-analysed[124] using a newly derived theoretical relativistic relationship between the γ-ray cross-section and the impulse Compton profile. Williams[125] has shown that this new derivation cannot be the correct relativistic one since when it is expressed in terms of the usual variables, it reduces essentially to the non-relativistic result. Thus we are left with a problem in interpreting experimental profiles obtained from experiments using γ-ray sources, as the experimental analyses have all used one form or another of an incorrect theoretical relationship to obtain the Compton profile from the experimental cross-section. However, it is expected that such errors will not be large. As we stated in the previous section, a new derivation of the correct relativistic relationship between cross-section and impulse Compton profile has recently been reported.[118] Only at very large incident energies (above 160 keV) and/or small scattering angles will the errors after normalization affect the profile to any appreciable extent. In particular Ribberfors[118] shows that for a scattering angle of 150° and incident photon energies up to 330 keV, the corrections will be negligible out to $q = 10$ a.u. after renormalization. It would be most interesting to see an analysis of the experimental data using Ribberfors' iterative procedure instead of the first approximation.

In the rest of this section theory and experiment for X-ray Compton scattering from neon will be compared and some of the apparent anomalies which have come out of the X-ray experiments on krypton will be discussed.

5.6.1 Neon

In Table 5.7[78] Eisenberger's experimental L-shell profiles for Mo $K\alpha$ and Ag $K\alpha$ X-rays scattering through 170° from neon are compared with EH profile calculations and five impulse calculations: one HF, one shielded hydrogenic, and three which include correlation effects. In the EH calculations, shielding factors $Z^*(0)$ in the $2s$ and $2p$ wave functions were chosen to match the impulse hydrogenic (IH) profiles for the individual states to the respective impulse Hartree–Fock (IHF) Compton

Table 5.7 Comparison of theoretical and experimental neon *L*-shell Compton profiles for Mo $K\alpha$ and Ag $K\alpha$ X-rays scattering through 170°

	Mo $K\alpha$		Impulse Calculations					Ag $K\alpha$	
q	EH[c]	EXP[a]	IH	IHF	ICI[b]	IBGI[d]	IMCHF[e]	EXP[a]	EH[c]
0·0	2·609	2·598	2·548	2·548	2·545	2·554	2·557	2·565	2·589
0·1	2·612	2·592	2·540	2·540	2·537	2·546	2·550	2·556	2·592
0·2	2·595	2·577	2·517	2·516	2·518	2·522	2·526	2·536	2·577
0·3	2·557	2·533	2·479	2·475	2·472	2·480	2·484	2·505	2·541
0·4	2·498	2·465	2·425	2·415	2·412	2·419	2·422	2·438	2·485
0·5	2·419	2·369	2·355	2·335	2·332	2·338	2·340	2·350	2·409
0·6	2·320	2·269	2·270	2·237	2·234	2·267	2·239	2·243	2·315
0·7	2·206	2·126	2·170	2·120	2·119	2·120	2·121	2·122	2·204
0·8	2·078	1·984	2·058	1·993	1·990	1·990	1·990	1·988	2·080
0·9	1·940	1·836	1·935	1·856	1·853	1·852	1·851	1·842	1·945
1·0	1·796	1·679	1·804	1·715	1·712	1·709	1·707	1·690	1·804

[a] The experimental *L*-shell data given in Ref. 78 was obtained by subtracting an EH type $1s^2$ core profile from the total experimental profile.

[b] Configuration interaction profile calculations of Smith and Brown[109] using the full second order CI function of Ref. 112.

[c] $Z^*_{2s}(0) = 5{\cdot}99$ and $Z^*_{2p}(0) = 4{\cdot}96$ were the effective charges used in these calculations.

[d] Profile calculation of Naon and Cornille using Nesbet's Bethe Goldstone increment method to treat *L*-shell correlation.[105]

[e] Profile calculation of Smith and Brown[109] using the *L*-shell MCHF function of Ahlrichs and Hinze.[113]

profiles at $q = 0$. With this choice of effective charge, it was found that the IH *L*-shell neon profiles agreed with the IHF profiles to three or more figures out to a q of about 0·3. In argon[99] a similar comparison of IHF with IH using $Z^*(0)$ values showed agreement of the 2*s* and 2*p* profiles to three significant figures or more out to a q greater than 1. Mendelsohn and Bloch[21] asserted that if one was interested in obtaining an accurate EH profile calculation in the neighbourhood of $q = 0$, it was most reasonable to use these same $Z^*(0)$ values which gave IH profiles in agreement with IHF profiles, not only at $q = 0$, but also in some neighbourhood of the profile centre. This appears to be the case for EH Mo $K\alpha$ calculations for q between 0 and 0·3, where the EH results lie much closer to the experimental profile than either of the two impulse calculations. At $q = 0$ the EH $J(0)$ result lies only 0·42 per cent above the experimental value. Since the experiment cites error bars of 1 per cent, the EH value falls well within the error bars. On the other hand the IHF $J(0)$ value lies 1·93 per cent below the Mo $K\alpha$ experimental results and therefore lies outside the experimental error bars. From the EH calculations the value of $J(0)$ decreases as the incident photon energy increases in agreement with experiment. The impulse profile calculation has no intrinsic dependence on incident photon energy and therefore can *never* explain such incident photon energy effects. We expect the IHF to fall closer to the Ag $K\alpha$ experimental results than the Mo $K\alpha$ ones because the IHF should improve in accuracy with increased photon energy. This is indeed observed to be the case. The Ag $K\alpha$ EH $J(0)$ value falls within the experimental error bars but appears to offer no real improvement to IHF. A possible explanation of this is given in Ref. 19.

We observe that all four impulse calculations lie within the experimental errors

at $q = 0$ and that the correlation effects on $J(0)$ are quite small. Eisenberger had previously compared his experimental results with an impulse profile calculated with a correlated wave function which contained errors and which gave a $J(0)$ value 0·75 *per cent* above the IHF result. This led him to conclude that improved agreement with experiment would be obtained when a better correlated wave function was used. However Table 5.7 shows that correlation effects on the Compton profile of neon are too small to be observed experimentally at this time or to decide the question of the sign of the correlation correction to the IHF peak value. As Table 5.7 reveals, the two wave functions which yield the largest correlation energy give the opposite sign for the correlation correction to the IHF profile peak. As we discussed in section 5.3, virial theorem scaling of the VHS peak value raises it slightly above the IHF one. Furthermore, the AH–MCHF and BGI calculations include only L-shell correlation while the VHS function included K, L, and K–L intershell correlation. In this case, the experimental procedure of subtracting the IHF core contribution was followed. Relativistic flattening of the neon profile which is not included in any of the calculations is also about 0.1 per cent.

Recently Bonham and associates[126] have performed experiments to determine the Compton profile of neon from the inelastic scattering of 25 keV *electrons*. (See chapter 8.) They find that the EH results lie closer than any impulse calculation to their experimental profile, in the vicinity of the profile centre, even though the EH results still appear to be about 2 per cent too low. They state,[126] 'the EH calculations which explicitly sum over all transitions to the excited ion states seem to present a better description of the experimental Compton process'.

The partial wave Hartree–Fock–Slater (Herman–Skillman) calculations of Grossman and Mendelsohn[25] on neon give the closest agreement with experiment for both small q (except for Mo $K\alpha$ scattering at $q = 0$ where EH gives the best result) and large q for both Mo $K\alpha$ and Ag $K\alpha$ Compton scattering. Of all the theoretical calculations, the EHS results are found to be in closest agreement with the experimental neon results over the whole profile.

Table 5.8 Comparison of theoretical and experimental Compton profiles for krypton. Experiment using 160 keV photons scattered through 173°

	Experiment		Theory	
q (a.u.)	Original[123]	Re-analysed[124]	IHF[79]	IDHF[79]
0·0	7·205	7·312	7·24	7·19
0·1	7·152	7·260	7·20	7·15
0·2	7·022	7·109	7·10	7·05
0·4	6·459	6·559	6·60	6·57
0·6	5·700	5·787	5·78	5·77
1·0	4·134	4·185	4·04	4·04
2·0	2·533	2·535	2·44	2·44
4·0	1·338	1·271	1·33	1·33
6·0	0·687	0·673	0·677	0·679
10·0	0·254	0·240	0·260	0·261
25·0	0·024		0·026	0·027

5.6.2 Krypton

In Table 5.8 the impulse non-relativistic Hartree–Fock (IHF) and the relativistic Dirac–Hartree–Fock (IDHF) calculations are compared with the original[123] and re-analysed[124] γ-ray results of Eisenberger and Reed. The only effects omitted from the IDHF calculation are binding effects and correlation effects. Clearly binding effects will be negligible at such high incident photon energies and large scattering angles. For this closed shell system correlation effects are expected to be quite small. Thus it appears that the re-analysed experimental results are in worse agreement with theory than the original results near the profile centre.

ACKNOWLEDGEMENTS

We would like to thank the United States Office of Naval Research (LBM) and the National Research Council of Canada (VHS) for their support.

REFERENCES

1. DuMond, J. W. M., 'Compton modified line structure and its relation to the electron theory of solid bodies', *Phys. Rev.*, **35**, 643, 1929.
2. DuMond, J. W. M., 'The linear momenta of electrons in atoms and solid bodies as revealed by X-ray scattering', *Rev. Mod. Phys.*, **5**, 1, 1933.
3. Cooper, M., 'Compton scattering and electron momentum distributions', *Adv. Phys.*, **20**, 453, 1971.
4. Epstein, I. R., 'Electron momentum distributions in atoms, molecules and solids', *MTP International Review of Science*, Physical Chemistry, Series II, Theoretical Chemistry, 145, 1975.
5. Waller, I. and D. R. Hartree, 'On the intensity of total scattering of X-rays', *Proc. Roy. Soc. A*, **124**, 119, 1929.
6. Eisenberger, P. and P. M. Platzman, 'Compton scattering of X-rays from bound electrons', *Phys. Rev. A*, **2**, 415, 1970.
7. Gavrila, M., 'Compton scattering by *K*-shell electrons. I. Nonrelativistic theory with retardation', *Phys. Rev. A*, **6**, 1348, 1972.
8. Gavrila, M., 'Compton scattering by *K*-shell electrons. II. Nonrelativistic dipole approximation', *Phys. Rev. A*, **6**, 1360, 1972.
9. Schwinger, J., *Quantum Electrodynamics*, New York, The derivation for the non-relativistic bound electron case follows closely along the lines of the free electron case to p. 21.
10. Phillips, W. C. and R. J. Weiss, 'X-ray determination of electron momenta in Li, Be, Na, Mg, Al and LiF', *Phys. Rev.*, **171**, 790, 1968.
11. Williams, B. G., 'Standardization of Compton profile measurements – The Compton profile of water', *Acta Cryst.*, **A32**, 513, 1976.
12. Mendelsohn, L. B., private communication.
13. Kilby, G. E., 'A wave mechanical derivation of the intensity distribution of the Compton line', *Proc. Phys. Soc.*, **86**, 1037, 1965.
14. Jones, W. and N. H. March, *Theoretical Solid State Physics, Volume 1: Perfect Lattices in Equilibrium*, Wiley-Interscience, London, 1973.
15. Benesch, R. and V. H. Smith, Jr., 'Density matrix methods in X-ray scattering and momentum

space calculations', in *Wave Mechanics—The First Fifty Years*, Price, W. C., S. S. Chissick, and T. Ravensdale, editors, Butterworths, London, 1973.
16. Smith, V. H., Jr., 'On the impulse approximation in Compton scattering from bound electrons', paper presented at the *International Symposium on Quantum Chemistry and Solid State Physics*, Bieto, Norway, 1972.
17. Gummel, H. and M. Lax, 'Thermal capture of electrons in silicon', *Ann. Phys. (N.Y.)*, **2**, 28, 1957.
18. Mendelsohn, L. B. and F. Biggs, 'K-shell Compton profiles and incoherent scattering factors', in *Inner-shell Ionization Phenomena and Future Applications*, Fink, R. W., editor, US Atomic Energy Conference 720404, **3**, 1142, 1973.
19. Mendelsohn, L. B., B. J. Bloch, and V. H. Smith, Jr., 'Incident X-ray energy dependence of neon Compton profiles', *Phys. Rev. Lett.*, **31**, 266, 1973.
20. Bloch, B. J. and L. B. Mendelsohn, 'Atomic L-shell Compton profiles and incoherent scattering factors: Theory', *Phys. Rev. A*, **9**, 129, 1974.
21. Mendelsohn, L. B. and B. J. Bloch, 'Atomic L-shell Compton profiles: Calculations for atoms and comparison with experiment', *Phys. Rev. A*, **12**, 551, 1975.
22. Nikolaev, V. S. and I. M. Kruglova, 'On qualitative features of generalized oscillator strengths and ionization cross sections in ion-atom collisions', *Phys. Lett. A*, **37**, 315, 1971.
23. Currat, R., P. D. DeCicco, and R. Kaplow, 'Compton scattering and electron momentum density in beryllium', *Phys. Rev. B*, **3**, 243, 1971.
24. Currat, R., P. D. DeCicco, and R. J. Weiss, 'Impulse approximation in Compton scattering', *Phys. Rev. B*, **4**, 4256, 1971.
25. Grossman, H. and L. B. Mendelsohn, 'Exact Hartree–Slater Compton profile calculations', *Bull. Am. Phys. Soc., II*, **20**, 680, 1975.
26. Herman, F. and S. Skillman, *Atomic Structure Calculations*, Prentice-Hall, Englewood Cliffs, N.J., 1963.
27. Manson, S. and J. W. Cooper, 'Photoionization in the soft X-ray range: Z dependence in a central potential model', *Phys. Rev.*, **165**, 126, 1968.
28. Sabin, J. R. and V. H. Smith, Jr., 'A new criterion for choice of the local exchange parameter α', to be published.
29. Smith, V. H., Jr., private communication.
30. Smith, V. H., Jr. and R. Benesch, 'Atomic helium in momentum space', contributed paper in *International Symposium on the Physics of One and Two-Electron Atoms*, Munich, 1968.
31. Benesch, R. and V. H. Smith, Jr., 'Natural orbitals in momentum space and correlated radial momentum distributions I. The ^1S ground state of Li^+', *Int. J. Quant. Chem.*, **45**, 131, 1971.
32. Benesch, R. and V. H. Smith, Jr., 'Radial momentum distributions for the ^2S ground state of the lithium atom', *Chem. Phys. Lett.*, **5**, 601, 1970.
33. Munch, D. and E. R. Davidson, 'Non-relativistic configuration interaction calculations for the ground state of the vanadium atom', *J. Chem. Phys.*, **63**, 980, 1975.
34. Benesch, R., S. R. Singh, and V. H. Smith, Jr., 'On the relationship of the X-ray form factor to the 1-matrix in momentum space', *Chem. Phys. Lett.*, **10**, 151, 1971.
35. Singh, S. R. and V. H. Smith, Jr., 'Behaviour of Hartree–Fock–Slater ($X\alpha$) atomic form factors and electron momentum distributions for two-, three- and four-electron ions', *Z. Physik*, **255**, 83, 1972.
36. Hylleraas, E. A., 'Die Wellengleichung des Keplerproblems im Impulsraume', *Z. Physik*, **74**, 216, 1932.
37. Fock, V., 'Zur Theorie des Wasserstoffatoms', *Z. Physik.*, **98**, 145, 1935.

38. Lévy, M., 'Wave equations in momentum space', *Proc. Roy. Soc.*, **204**, 145, 1950.
39. McWeeny, R. and C. A. Coulson, 'The computation of wave functions in momentum space I. The helium atom', *Proc. Phys. Soc.*, **A62**, 509, 1949.
40. Henderson, M. G. and C. W. Scherr, 'Helium wave function in momentum space', *Phys. Rev.*, **120**, 150, 1960.
41. Löwdin, P.-O., 'Quantum theory of many-particle systems I. Physical interpretation by means of density matrices, natural spin orbitals and convergence problems in the method of configurational interaction', *Phys. Rev.*, **97**, 1474, 1955.
42. Smith, V. H., Jr. and J. E. Harriman, 'A proposal concerning terminology in reduced density matrix theory', *Technical Report*, WIS-TCI-379, Theoretical Chemistry Institute, University of Wisconsin, 1970.
43. Larsson, S. and V. H. Smith, Jr., 'Natural spin orbitals and geminals for the lithium ^2S ground state', *Int. J. Quant. Chem.*, **6**, 1019, 1972.
44. Bonham, R. A., private communication.
45. Benesch, R., 'Momentum distributions and Compton profiles from two-electron atomic wave functions containing exponential correlation terms', *J. Phys. B*, to be published.
46. Benesch, R., 'Algebraic I-matrices and radial momentum distributions from Hylleraas-type wave functions. ^1S ground states of He and He-like ions', *Phys. Rev. A*, **6**, 573, 1972.
47. Hicks, B., 'The shape of the Compton modified line for helium and molecular hydrogen', *Phys. Rev.*, **52**, 436, 1937.
48. Podolsky, B. and L. Pauling, 'The momentum distribution in hydrogen-like atoms', *Phys. Rev.*, **34**, 109, 1929.
49. Kaijser, P. and V. H. Smith, Jr., 'Evaluation of momentum distributions and Compton profiles for atomic and molecular systems', *Adv. Quant. Chem.*, to be published.
50. Thakkar, A. and V. H. Smith, Jr., 'A strategy for the numerical evaluation of Fourier sine and cosine transforms', *Comput. Phys. Comm.*, **10**, 73, 1975.
51. Benesch, R., 'Fourier transformation of tabulated functions', to be published.
52. Thulstrup, P. W., 'Smooth interpolation, Fourier transformation and two-centre overlap integrals for numerical atomic orbitals', *Int. J. Quant. Chem.*, **9**, 789, 1975.
53. Bethe, H. A. and E. E. Salpeter, *Quantum Mechanics of One and Two-Electron Atoms*, Academic Press, New York, 1957.
54. Wellenstein, H. F., R. A. Bonham, and R. C. Ulsh, 'Bethe surface and inelastic and elastic differential cross sections for helium obtained by the use of 25 keV incident electrons', *Phys. Rev. A*, **8**, 304, 1973.
55. Epstein, I. R., 'Calculation of atomic and molecular momentum expectation values and total energies from Compton scattering data', *Phys. Rev. A*, **8**, 160, 1973.
56. Bonham, R. A., private communication.
57. Benesch, R. and V. H. Smith, Jr., to be published.
58. Kimball, J. C., 'Short-range correlations and the structure factor and momentum distribution of electrons', *J. Phys. A*, **8**, 1513, 1975.
59. Kato, T., 'On the eigenfunctions of many-particle systems in quantum mechanics', *Commun. Pure Appl. Math.*, **10**, 151, 1957.
60. Smith, V. H., Jr., 'Cusp conditions for natural functions', *Chem. Phys. Lett.*, **9**, 365, 1971.
61. Thakkar, A. J. and V. H. Smith, Jr., 'The electron-electron cusp condition for the spherical average of the intracule matrix', *Chem Phys Lett.*, **42**, 476, 1976.
62. Benesch, R. and V. H. Smith, Jr., 'Exact and asymptotic X-ray intensity values from 20-parameter Hylleraas-type wave functions: He and He-like ions', *Int. J. Quant. Chem.*, **5S**, 35, 1971.
63. (a) Pekeris, C. L., 'Ground state of two-electron atoms', *Phys. Rev.*, **112**, 1649, 1958.

(b) Accad, Y., C. L. Pekeris, and B. Schiff, '*S* and *P* states of the helium isoelectronic sequence up to $Z = 10$', *Phys. Rev.*, **4**, 516, 1971.
(c) Thakkar, A. J., and V. H. Smith, Jr., 'Compact and accurate integral transform wave functions I. The 1^1S state of helium-like ions from H^- through Mg^{10+}', *Phys. Rev. A*, to be published.
64. Weiss, R. J., 'X-ray Compton profiles of benzene, cyclohexane and oriented polyethylene', *J. Chem. Phys.*, **52**, 2237, 1970.
65. Burkhardt, G., 'Über die Form der Comptonlinie', *Ann. d. Phys.* (5), **26**, 567, 1936.
66. Kirkpatrick, P., P. A. Ross, and H. O. Ritland, 'Characteristics of the Compton modified band', *Phys. Rev.*, **50**, 928, 1936.
67. Hughes, A. L. and M. M. Mann, Jr., 'A new method for investigating atomic electron velocities', *Phys. Rev.*, **53**, 50, 1938.
68. Slater, J. C., 'Atomic shielding constants', *Phys. Rev.*, **36**, 57, 1930.
69. Duncanson, W. E. and C. A. Coulson, 'Theoretical Shapes of the Compton profile for atoms from H to Ne', *Proc. Phys. Soc.*, **57**, 190, 1945.
70. Duncanson, W. E. and C. A. Coulson, 'Electron momenta in atoms', *Proc. Phys. Soc.*, **60**, 175, 1948.
71. Duncanson, W. E. and C. A. Coulson, 'Atomic wave functions for ground states of elements Li to Ne', *Proc. Roy. Soc. Edin.*, **62A**, 37, 1944.
72. Clementi, E., 'Tables of atomic wave functions', *IBM J. Res. Dev. Supp.*, **9**, 2, 1965.
73. Froese-Fischer, C., 'A multi-configuration Hartree–Fock program with improved stability', *Comput. Phys. Commun.*, **4**, 107, 1972.
74. Weiss, R. J., A. Harvey, and W. C. Phillips, 'Compton line shapes for Hartree–Fock wave functions', *Phil. Mag.*, **17**, 241, 1968.
75. Naon, M., M. Cornille, and M. Roux, 'Compton profiles for the first and second row atoms', *J. Phys. B*, **4**, 1593, 1971.
76. Naon, M. and M. Cornille, '*Correlation effects in X-rays and electronic intensities for the neon atom*', *J. Phys. B*, **4**, 1210, 1971.
77. Smith, V. H., Jr., and M. H. Whangbo, 'Localized molecular orbital studies in momentum space I. Compton profiles of 1s core electrons and hydrocarbons', *Chem. Phys.*, **5**, 234, 1974.
78. Eisenberger, P., W. H. Henneker, and P. E. Cade, 'Compton scattering of X-rays from Ne, N_2 and O_2: A comparison of theory and experiment', *J. Chem. Phys.*, **56**, 1207, 1972.
79. (a) Biggs, F., L. B. Mendelsohn, and J. B. Mann, 'Hartree–Fock Compton profiles for the elements', *Atomic Data and Nuclear Data Tables*, **16**, 201, 1975.
(b) Biggs, F., L. B. Mendelsohn, and J. B. Mann, 'Relativistic orbital and entire-atom Compton profiles for the elements', *Sandia Report*, 75-0636, Sandia Laboratories, 1976.
80. Benesch, R., 'Compton profiles from numerical Hartree–Fock wave functions', *Can. J. Phys.*, to be published.
81. Smith, V. H., Jr., R. E. Brown, and R. Benesch, 'Compton profiles for non-closed shell atomic states: Boron (^2P)', to be published.
82. Bagus, P. and T. Gilbert, in McLean, A. D. and M. Yoshimine, 'Table of linear molecule wave functions', *IBM. J. Res. Dev. Supp.*, **12**, 206, 1968.
83. Smith, V. H., Jr., 'Theoretical aspects of Compton profiles', *Invited lecture, International Symposium on Atomic, Molecular and Solid State Physics in Honour of E. U. Condon*, Sanibel Island, Florida, 1973.
84. Kónya, A., 'Theoretische Berechnung der Form und Breite der Compton-linie', *Acta Phys. Hung.*, **1**, 12, 1949.
85. Coulson, C. A. and N. H. March, 'Momenta in atoms using the Thomas–Fermi method', *Proc. Phys. Soc. A.*, **63**, 367, 1950.

86. March, N. H., 'Momentum distribution of electrons in solids: results for some metals using the Thomas–Fermi method', *Proc. Phys. Soc. A*, **67**, 9, 1954.
87. March, N. H., 'The Thomas–Fermi approximation in quantum mechanics', *Adv. Phys.*, **6**, 1, 1957.
88. Lam, L. and P. Platzman, 'Momentum density and Compton profile of the inhomogeneous interacting electron system: application to atoms', *Phys. Rev. B*, **9**, 5128, 1974.
89. Palinkás, G., 'Compton intensities of heavy ions and Compton profiles of atoms, in the free Fermi gas approach', *Acta Cryst. A*, **31**, S229, 1975.
90. Slater, J. C., 'Statistical exchange-correlation in the self consistent field', *Adv. Quant. Chem.*, **6**, 1, 1972.
91. Hohenberg, P. C. and W. Kohn, 'Inhomogeneous electron gas', *Phys. Rev.*, **136**, B864, 1964.
92. Hedin, L. and S. Lundqvist, 'Effects of electron-electron and electron-phonon interactions on one-electron states of solids', *Solid State Physics*, **23**, 1, 1969.
93. Slater, J. C., 'A simplification of the Hartree–Fock method', *Phys. Rev.*, **81**, 385, 1951.
94. Euwema, R. N. and G. T. Surratt, 'Dependence of atomic Compton profiles upon the $X\alpha$ exchange parameter', *J. Phys. C*, **7**, 3655, 1974.
95. Sabin, J. R. and S. B. Trickey, 'Comparison of atomic Compton profiles obtained from four model local density functionals', *J. Phys. B*, **8**, 2593, 1975.
96. McNaughton, D. J. and V. H. Smith, Jr., 'An investigation of the Kohn–Sham and Slater approximations to the Hartree–Fock exchange potential', *Int. J. Quant. Chem.*, **3S**, 775, 1970.
97. Gaspar, R., 'On approximation to the Hartree–Fock potential by a universal potential function', (in German), *Acta Phys. Hung.*, **3**, 263, 1954.
98. Kohn, W. and L. J. Sham, 'Self-consistent equations including exchange and correlation effects', *Phys. Rev.*, **140**, A1133, 1965.
99. Bloch, B. J. and L. B. Mendelsohn, 'Comparison of methods for calculating atomic shielding factors', *Phys. Rev. A*, **12**, 1197, 1975.
100. Löwdin, P.-O., 'Correlation problems in many-electron quantum mechanics I. Review of different approaches and discussion of some current ideas', *Adv. Chem. Phys.*, **2**, 207, 1959.
101. Brillouin, L., 'La méthode du champ self-consistent', *Actual. Sci. Ind.*, **71**, 159, 1933.
102. Moller, C. and M. S. Plesset, 'Note on approximation treatment for many-electron systems', *Phys. Rev.*, **46**, 618, 1934.
103. Kutzelnigg, W. and V. H. Smith, Jr., 'Lower bounds for the eigenvalues of first-order density matrices', *J. Chem. Phys.*, **42**, 2791, 1965.
104. Weiss, R. J., 'Charge density and momentum density—a comparison between theory and experiment', *Acta Cryst. A*, **25**, 248, 1969.
105. Eisenberger, P., 'Electron momentum density of He and H_2: Compton X-ray scattering', *Phys. Rev. A*, **2**, 1078, 1970.
106. Benesch, R. and V. H. Smith, Jr., 'Scattering factors for atomic lithium from correlated and independent particle model wave functions', *J. Chem. Phys.*, **52**, 1466, 1970.
107. Benesch, R. and V. H. Smith, Jr., 'Radial momentum distributions $I(p)$ and Compton profiles $J(q)$. The ^1S Be atom ground state', *Phys. Rev. A*, **5**, 114, 1972.
108. Naon, M. and M. Cornille, 'Correlated radial momentum distributions $I(p)$ and Compton profiles $J(q)$. The (^1S) Be and (^1S) Ne atoms ground states', *J. Phys. B*, **6**, 954, 1973.
109. Smith, V. H., Jr. and R. E. Brown, 'Electron correlation and the Compton profile of atomic neon', *Chem. Phys. Lett.*, **20**, 424, 1973.
110. Brown, R. E. and V. H. Smith, Jr., 'Discrepancy between theory and experiment for the Compton profiles of molecular hydrogen', *Phys. Rev. A*, **5**, 140, 1972.

111. Smith, V. H., Jr., G. H. F. Diercksen, and W. P. Kraemer, 'The influence of electron correlation on the Compton profile of H_2O', *Phys. Lett.*, **54A**, 319, 1975.
112. Viers, W., F. E. Harris, and H. F. Schaeffer, III, 'Pair correlations and the electronic structure of neon', *Phys. Rev. A*, **1**, 24, 1970.
113. Ahlrichs, R. and J. Hinze, unpublished data.
114. Schaeffer, H. F. III, R. A. Klemm, and F. E. Harris, 'Atomic hyperfine structure II. First order wave functions for the ground states of B, C, N, O', *Phys. Rev.*, **181**, 137, 1969.
115. Brown, R. E. and V. H. Smith, Jr., 'One-electron reduced density matrices for Li (^2P) and B (^2P)', *Phys. Rev. A*, **3**, 1858, 1971.
116. Sinanoğlu, O., 'New atomic structure theory and beam-foil spectroscopy', *Rev. Mex. Fis.*, **20**, 143, 1971.
117. Clementi, E. and A. Veillard, 'Correlation effects in atomic systems IV. Degeneracy effects', *J. Chem. Phys.*, **44**, 3050, 1966.
118. Ribberfors, R., 'Relationship of the relativistic Compton cross section to the momentum distribution of bound electron states', *Phys. Rev. B*, **12**, 2067, 1975.
119. Mendelsohn, L. B., F. Biggs, and J. B. Mann, 'Relativistic Hartree–Fock Compton profiles', *Int. J. Quant. Chem.*, **57**, 395, 1973.
120. Mendelsohn, L. B., F. Biggs, and J. B. Mann, 'Relativistic Hartree–Fock Compton profiles for the rare gases and lead', *Chem. Phys. Lett.*, **26**, 521, 1974.
121. Mann, J. B. and J. T. Waber, 'Numerical relativistic Hartree–Fock wave functions', *Atomic Data*, **5**, 201, 1975.
122. Eisenberger, P., 'Compton profile measurements of N_2, O_2 and Ne using silver and molybdenum X-rays', *Phys. Rev. A*, **5**, 628, 1972.
123. Eisenberger, P. and W. A. Reed, 'γ-Ray Compton scattering: Experimental Compton profiles for He, N_2, Ar and Kr', *Phys. Rev. A*, **5**, 2085, 1972.
124. Eisenberger, P. and W. A. Reed, 'Relationship of the relativistic Compton cross section to the electron's velocity distribution', *Phys. Rev. B*, **9**, 3237, 1974.
125. Williams, B. G., private communication.
126. Wong, T. C., J. S. Lee, H. F. Wellenstein, and R. A. Bonham, 'Experimental definition of Compton profiles from 25 keV electron impact studies on N_2, Ne and Ar', *Phys. Rev. A*, **12**, 1846, 1975.